Forschungszentrum Karlsruhe
Technik und Umwelt

Wissenschaftliche Berichte
FZKA 6669

Linear and Nonlinear Interface Model Based on the Electric Double Layer Theory

G. Janssens-Maenhout, T. Schulenberg

Institut für Kern- und Energietechnik
Programm Mikrosystemtechnik

März 2002

Forschungszentrum Karlsruhe

Technik und Umwelt

Wissenschaftliche Berichte

FZKA 6669

Linear and Nonlinear Interface Model Based on the Electric Double Layer Theory

G. Janssens-Maenhout, T. Schulenberg

Institut für Kern- und Energietechnik
Programm Mikrosystemtechnik

Forschungszentrum Karlsruhe GmbH, Karlsruhe
2002

Als Manuskript gedruckt

Forschungszentrum Karlsruhe GmbH
Postfach 3640, 76021 Karlsruhe

Mitglied der Hermann von Helmholtz-Gemeinschaft
Deutscher Forschungszentren (HGF)

ISSN 0947-8620

Abstract

Aqueous solutions and liquid metals in contact with other phases or components experience strong Coulomb forces at their interface. To account this effect an electrical double layer at these liquid interfaces is introduced in the classical fluid dynamics. Coupling the electrostatic equations with the hydrodynamic equations, a microscopic model for a surface layer of finite thickness is developed. The model is based on an infinitely thin layer right at the surface, which includes all molecular surface effects empirically and a layer of finite thickness next to it, in which ions are distributed according to a Boltzmann function. A validation is performed by comparing the analytical results for the surface tension with experimental findings for the contact angle of liquid droplets on a solid surface, and the pressure drop in a micro channel.

Mikroskopisches Modell aus der elektrischen Doppelschichttheorie zur linearen und nichtlinearen Beschreibung der Grenzfläche

Zusammenfassung

Wässrige Lösungen und Flüssigmetalle in Kontakt mit anderen Phasen oder Komponenten weisen starke Coulombkräfte an der Grenzfläche auf. Ein neues Modell für die Oberflächenspannung an Grenzflächen zwischen Flüssigkeit/Gas, Flüssigkeit/Flüssigkeit oder Flüssigkeit/Festkörper wird diskutiert, das diese Coulombkräfte an der Grenzfläche beschreibt. Dazu wird eine elektrische Doppelschicht modelliert. Mit der analytischen Lösung der nichtlinearen Poisson-Boltzmann-Gleichung wird die Oberflächenenergie verschiedener flüssig/gas, flüssig/flüssig und flüssig/fest Systeme berechnet und eine Beziehung für den Kontaktwinkel eines fest/flüssig/gas Systems hergeleitet. Dieses Modell wird weiter angewandt zur Druckverlust-Berechnung einer Kapillar- oder Oberflächenspannungsgetriebenen Strömung in einem Mikrosystem.

Contents

Chapter 1

Introduction.

The recent progress in manufacturing technologies for micro-systems has raised the question of how accurate classical fluid dynamic theory predicts the flow through microchannels. Flows in microchannels, which we define as channels with a diameter < 100 μm, are to be carefully investigated for the "laboratory on the chip". As an example the improvement of detection and separation processes in the chromatography or electrochemistry needs to analyze the flow and mixing of small amounts of complex fluid molecules. Microchannel flows differ from those in macroscopic channels basically in the following three features:

- The Reynolds number is lower and therefore the flow is laminar or even of Stokes type, i.e. without inertia. Care is needed, however, with the projection of the well-known macroscopic laws on the flow in a microchannel. According to Obot (2000) experimental observations indicate a different flow structure in microchannels with e.g. an earlier onset of transition to turbulent flow at Re $\approx$ 1000.

- Averaging with a smaller characteristic length scale give rise to microscopic effects and even induce invalidity of the continuum approach in the limit of molecular length scales.

- Capillary forces influence or even dominate the flow.

Whereas the first feature simplifies the analysis and the second feature marks the low er limit for continuum mechanics, we find a number of open questions about the last feature. Already 200 years ago, Young (1805) noticed that a surface tension not only exists at a gas / liquid interface, but also at a liquid / solid interface. The common understanding at that time was that surface tension acts in a layer of zero thickness. On the other hand, no-slip as boundary condition was assumed for the fluid dynamic equation by Navier and Stokes. Consequently, single-phase capillary forces could not drive the flow.
By the end of the 19th century, Van der Waals (1893) and Rayleigh (1892) built up the statistical thermodynamic theory of a diffuse interface. Helmholtz (1879) was the first to realize that an electrode immersed in a solution of an electrolyte is surrounded by a zone of ions predominantly of opposite charge, forming a double layer. Gouy (1910) and Chapman (1913) assumed that the size of these ions is negligible, compared to their distances, and that the causing mechanism is the opposing electric effect of both the attractive Coulomb

forces between the ions and the wall and the repulsive Coulomb forces between the ions themselves. Their theory, characterizing these surface layers, became known as electric double layer (EDL). Stern (1924) improved this theory by the recognition that the nonzero size of the ions prevented their centers from reaching the surface of the electrode and that an adsorbed layer of counter-ions exists, known as Stern layer.
It wasn't until the end of the 20th century that the theory of the EDL was applied to fluid dynamics. Lozada-Cassou (1992) and Mala, Li and Dale (1996) succeeded to predict a flow of an electrolyte through microchannels formed by electrodes. The EDL field in such a microchannel, governed by the two-dimensional nonlinear Poisson-Boltzmann equation is solved by Mala, Yang and Li (1998) in two ways: either analytically with the use of the Debye-Hückel linear approximation or numerically without any approximation. They demonstrated that the EDL causes an additional pressure drop compared with predictions of the Navier-Stokes equation. Even though their results are restricted to walls with a given surface potential, and later experiments of Mala and Li (1999) could not confirm the analyses, we still consider their approach to be the key to micro fluid dynamics. Hu, Harrison and Masliyah (1999) followed a similar approach and developed a numerical model for electrokinetic flow.
With the present paper we generalize the theory of the EDL to all kinds of liquid surfaces. Care has been taken to base the theory only on measurable, macroscopic properties to ease its application. Like in the EDL-theory, Coulomb forces are taken into account in a layer of nonzero thickness. The Van der Waals forces act within much smaller range than the Coulomb forces (r^{-6} instead of r^{-2}). Their influence is restricted to a layer of a few nanometers thickness at the surface, which we include only as an integral quantity right at the surface in our model. Forces of chemical character, e.g. hydration forces and steric forces are omitted for simplicity. As a consequence, the theory is restricted to liquids composed of ions such as water, aqueous solutions of salts, bases and acids, or liquid metals. It is the aim of the EDL model to interpret Coulomb forces in surface layers of a finite thickness as a part of the capillary forces. The coupling of the fluid motion and the electric field is covered by electrohydrodynamics, as described by Melcher and Taylor (1969). Here, the Poisson-Boltzmann equation is solved analytically and without use of the Debye-Hückel-approximation. This approach should enable us to predict some typical flow phenomena in microchannels such as the increased pressure drop of liquid flows or other effects, which cannot be predicted by the Navier-Stokes equation in its classical form. The recent progress in manufacturing technologies for micro-systems has raised the question of how accurate classical fluid dynamic theory predicts the flow through microchannels. Flows in microchannels, which we define as channels with a diameter < 100 μm, differ from those in macroscopic channels basically in the following three features:

- The Reynolds number is lower and therefore the flow is laminar or even Stokes flow, i.e. without inertia. Care is needed, however, with the projection of the well-known macroscopic laws on the flow in a microchannel. According to Obot (2000) experimental observations indicate a different flow structure in microchannels with e.g. an earlier onset of transition to turbulent flow at $\mathrm{Re} \approx 1000$.

- Averaging with a smaller characteristic length scale give rise to microscopic effects and even induce invalidity of the continuum approach in the limit of molecular length

scales.

- Capillary forces influence or even dominate the flow. Whereas the first feature simplifies the analysis and the second feature marks the lower limit for continuum mechanics, we find a number of open questions about the last feature.

Already 200 years ago, Young (1805) noticed that a surface tension not only exists at a gas / liquid interface, but also at a liquid / solid interface. The common understanding at that time was that surface tension acts in a layer of zero thickness. On the other hand, no-slip as boundary condition was assumed for the fluid dynamic equation by Navier and Stokes. Consequently, single-phase capillary forces could not drive the flow.
By the end of the 19th century, Van der Waals (1893) and Rayleigh (1892) built up the statistical thermodynamic theory of a diffuse interface. Helmholtz (1879) was the first to realize that an electrode immersed in a solution of an electrolyte is surrounded by a zone of ions predominantly of opposite charge, forming a double layer. Gouy (1910) and Chapman (1913) assumed that the size of these ions is negligible, compared to their distances, and that the causing mechanism is the opposing electric effect of both the attractive Coulomb forces between the ions and the wall and the repulsive Coulomb forces between the ions themselves. Their theory, characterizing these surface layers, became known as electrical double layer (EDL). Stern (1924) improved this theory by the recognition that the nonzero size of the ions prevented their centers from reaching the surface of the electrode and that an adsorbed layer of counter-ions exists, known as Stern layer.
It wasn't until the end of the 20th century that the theory of the EDL was applied to fluid dynamics. Lozada-Cassou (1992) and Mala et al. (1996) succeeded to predict a flow of an electrolyte through microchannels formed by electrodes. The EDL field in such a microchannel, governed by the two-dimensional nonlinear Poisson-Boltzmann equation is solved by Mala et al. (1998) in two ways: either analytically with the use of the Debye-Hückel linear approximation or numerically without any approximation. They demonstrated that the EDL causes an additional pressure drop compared with predictions of the Navier-Stokes equation. Even though their results are restricted to walls with a given surface potential, and later experiments of Mala and Li (1999) could not confirm the analyses, we still consider their approach to be the key to micro fluid dynamics. Hu et al. (1999) followed a similar approach and developed a numerical model for electrokinetic flow.
With the present paper we like to generalize the theory of the EDL to all kind of liquid surfaces. Care has been taken to base the theory only on measurable, macroscopic properties to ease its application. Like in the EDL-theory, Coulomb forces are taken into account in a layer of nonzero thickness. The van der Waals forces act within much smaller range than the Coulomb forces (r^{-6} instead of r^{-2}). Their influence is restricted to a layer of a few nanometers thickness at the surface, which we include only as an integral quantity right at the surface in our model. Forces of chemical character, e.g. hydration forces and steric forces are omitted for simplicity. As a consequence, the theory is restricted to liquids composed of ions such as water, aqueous solutions of salts, bases and acids, or liquid metals. It is the aim of the EDL model to interpret Coulomb forces in surface layers of a finite thickness as capillary forces. The coupling of the fluid motion and the electrical field is covered by electrohydrodynamics, as described by Melcher and Taylor (1969). Here, the

Poisson-Boltzmann equation is solved analytically and without use of the Debye-Hückel-approximation. This approach should enable us to predict some typical flow phenomena in microchannels such as the increased pressure drop of liquid flows or other effects, which cannot be predicted by the Navier-Stokes equation in its classical form.

Chapter 2

Microscopic Interface Model.

2.1 Model Assumptions.

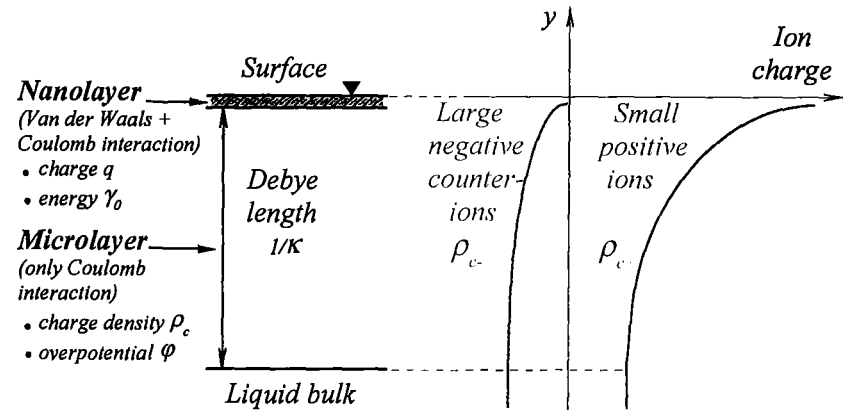

Figure 2.1: Model assumption of the liquid interface composed of a nanolayer at the surface and an electric microlayer underneath.

The liquid interface to gases, solids or other immiscible liquids is considered to be composed of a "nanolayer" of a few molecular dimensions size, right at the interface, and a "microlayer" of the order of a micrometer thickness underneath. The nanolayer shall include all molecular effects, like the concentration of charged ions or the alignment of dipoles at the surface, which are caused by the complex interaction of Van der Waals forces and Coulomb forces and which can be described by a Mie pair potential such as the Lennard-Jones potential function. As we try to keep the model simple, we will not describe this nanolayer based on its molecular properties. Instead, we condense it to an infinitely thin layer like in the classical capillary theory. All we need to know about this nanolayer is then

- its integral charge density, later on referred to as the surface charge density q, and
- its surface energy density γ_0.

These two properties will be determined empirically. So far, the nanolayer is a kind of generalized Stern layer of the classical EDL-theory.
The microlayer extends from the surface till the bulk of the fluid, but does not contain the nanolayer at the surface. It is equivalent to the electric double layer used by Gouy and Chapman. We assume that the liquid contains positive and negative ions which are small compared with their distances from each other, so that we can approximate them as point ions. This assumption is valid for water, aqueous solutions of salts, acids or bases, which have traditionally been considered in the EDL-theory. Moreover, we can include liquid metals in which the free electrons are distributed similarly.
Ions in the microlayer are not uniformly embedded within counter-ions. According to Israelachvili (1998) the interaction of these point ions with themselves and with counter-ions results in a Boltzmann distribution for the ion density. Thereby the charge density is coupled with the local potential, which we call the overpotential, to distinguish it from an externally applied potential later on[1]. The Boltzmann distribution yields a charge density ρ_{ci} of each set i of ions, given by

$$\rho_{ci} = z_i e n_{i\infty} \exp(-\frac{z_i e\, \varphi}{kT}) \quad . \tag{2.1}$$

Here, z_i is the valence of the ions, e the magnitude of electron charge, $n_{i\infty}$ the ion concentration of set i in the bulk of the liquid, φ the local overpotential, k the Boltzmann constant, and T the absolute temperature of the liquid. The resulting charge density ρ_c is composed of the ion and counter-ion charge densities ρ_{ci} in the microlayer and is given by the sum

$$\rho_c = \sum_i \rho_{ci} = \sum_i z_i e n_{i\infty} \exp(-\frac{e\, z_i \varphi}{kT}) \quad . \tag{2.2}$$

In the bulk, the ions and counter-ions are uniformly distributed and compensate each other electrically, so that for $\varphi \to 0$:

$$\sum_i z_i n_{i\infty} = 0 \quad . \tag{2.3}$$

Under the assumption of a small overpotential φ

$$\frac{z_i e\, \varphi}{kT} << 1 \quad , \tag{2.4}$$

the charge density ρ_c can be linearized as

$$\rho_c \approx -\frac{\varphi}{kT} \sum_i z_i^2 e^2 n_{i\infty} \quad . \tag{2.5}$$

This approximation, called the Debye-Hückel linear approximation, is only applicable if the overpotential φ is smaller than 25 mV. In practice, most solid / liquid surfaces have a surface electrical overpotential larger than 25 mV, so that no linearized solution can be applied. However, this report treats also the linearized problem,because of the physical insights under mathematical simplicity.

[1]This nomenclature has recently been introduced by Dahlkild (2001). In electrochemistry no specific name for this potential is used by e.g. Israelachvili (1998) or Grossman (1992). In Magneto Hydrofluid Dynamics however, Blums, Mikhailov and Ozols (1987) calls this potential the overvoltage.

2.2 Electrostatics.

The Maxwell equation relates to the charge ρ_c an electric field $\vec{\mathbf{E}}$ with the dielectric constant of the fluid ε and with the permittivity of free space ε_0:

$$\varepsilon\varepsilon_0 \vec{\nabla} \cdot \vec{\mathbf{E}} = \rho_c \quad . \tag{2.6}$$

With $\vec{\mathbf{E}} = -\vec{\nabla}\varphi$, for a quasi-steady state electric field, Eq. (2.6) leads to the Poisson equation[2]

$$\Delta\varphi = -\frac{\rho_c}{\varepsilon\varepsilon_0} \quad . \tag{2.7}$$

Substitution of Eq. (2.2) in Eq. (2.7) yields the nonlinear Poisson-Boltzmann equation:

$$\Delta\varphi = -\sum_i \frac{z_i e n_{i\infty}}{\varepsilon\varepsilon_0} \exp(-\frac{e\, z_i\, \varphi}{kT}) \quad . \tag{2.8}$$

At the interface, the charge density of the nanolayer q acts like the surface of a capacitor plate. It induces an electric field $\vec{\mathbf{E}}$ with a component normal to the surface at position $\vec{\mathbf{o}}$, given by

$$E_n\,(\vec{\mathbf{x}}=\vec{\mathbf{o}}) = -\frac{q}{\varepsilon\varepsilon_0} \quad . \tag{2.9}$$

This Eq. (2.9) determines the following boundary condition for the gradient of the electric overpotential φ of Eq. (2.7) normal to the surface

$$\frac{\partial\varphi}{\partial n}\,(\vec{\mathbf{x}}=\vec{\mathbf{o}}) = \frac{q}{\varepsilon\varepsilon_0} \quad . \tag{2.10}$$

Thereby $\vec{\mathbf{n}}$ is defined as the normalized vector, perpendicularly pointing outside the flow area. This definition fixes the sign of φ for given q. With boundary condition (2.10), the electroneutrality constraint over both surface layers is fulfilled:

$$q + \int_0^{+\infty} \rho_c \, dn = 0 \quad . \tag{2.11}$$

For simplicity this report will concentrate on symmetrically polyvalent liquids with positive ions of valence $+z$ and negative ions of valence $-z$. For these kind of polyvalent liquids Eq. (2.8) becomes

$$\Delta\varphi = \varkappa^2 \frac{kT}{ze} \sinh(\frac{ze\,\varphi}{kT}) \quad , \tag{2.12}$$

with

$$\varkappa^2 = \frac{2z^2e^2n_\infty}{\varepsilon\varepsilon_0 kT} \tag{2.13}$$

as Debye-Hückel-parameter. In general, the Debye-Hückel-parameter of polyvalent liquids would be defined as

$$\varkappa^2 = \frac{\sum_i z_i^2 e^2 n_{i\infty}}{\varepsilon\varepsilon_0 kT} \quad . \tag{2.14}$$

[2]Note that the Poisson equation allows to write the charge density in the fluid as $\rho_c = -\varepsilon\varepsilon_0\Delta\varphi$, which will be used in the non-linear approach.

The inverse of this parameter, $\varkappa^{-1}$, with the dimension of a length is called the Debye length and characterizes the thickness of the microlayer. As an example, the Debye length of water is 966 nm. Fig. (2.2) illustrates that the Debye length of aqueous solutions decreases significantly with increasing salt concentrations.

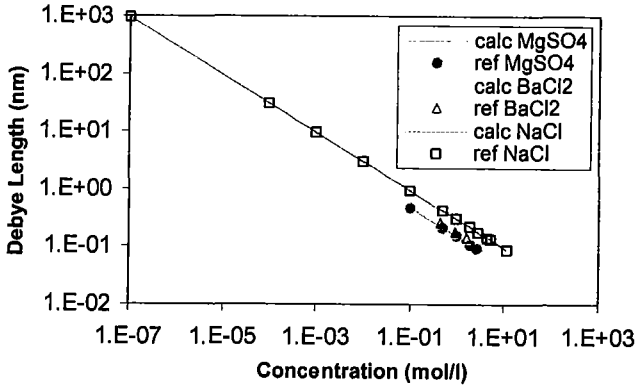

Figure 2.2: Comparison of the Debye length calculated with Eq. (2.14) (noted as calc) and the Debye length calculated with a correlation of Israelachvili (1998) as function of the concentration (noted as ref).

2.3 Equations of Motion.

The momentum conservation for a homogenous, Newtonian liquid with constant kinematic viscosity ν, constant density ρ and velocity $\vec{\mathbf{w}}$ is given by the Navier-Stokes equation, which has been extended by the electrodynamic force:

$$\rho\left(\frac{\partial}{\partial t}\vec{\mathbf{w}} + \vec{\mathbf{w}}\cdot\vec{\nabla}\vec{\mathbf{w}}\right) = \rho\vec{\mathbf{g}} - \vec{\nabla}p + \rho\nu\Delta\vec{\mathbf{w}} + \rho_c\vec{\mathbf{E}} \quad . \tag{2.15}$$

Here, $\rho\vec{\mathbf{g}}$ represents the gravity force, $\vec{\nabla}p$ the pressure gradient, $\rho\nu\Delta\vec{\mathbf{w}}$ the friction and additionally $\rho_c\vec{\mathbf{E}} = -\rho_c\vec{\nabla}\varphi$ the Coulomb forces[3].
The continuity equation reads for incompressible fluids:

$$\vec{\nabla}\cdot\vec{\mathbf{w}} = 0 \quad . \tag{2.16}$$

The scope of this report is restricted to isothermal flows with constant bulk concentrations, even though the model assumptions are not limited to these cases. Appropriate boundary conditions and closure relations are derived in the following sections.

[3]The Lorentz-force has been neglected, because for a given electrical field the magnetic field is of the order $\mu_0\varepsilon_0 = c^{-2}$ smaller.

2.4 Scaling.

In the following we concentrate on the one-dimensional case of a fluid in equilibrium and a plane surface with y as normal direction. We use an asterix as index to indicate dimensionless variables. If we scale the overpotential by

$$\varphi^* = \frac{\varphi}{kT/(ze)} \quad , \tag{2.17}$$

and the boundary layer coordinate by

$$y^* = \frac{y}{1/\varkappa} \quad , \tag{2.18}$$

we find the nondimensional equation for the scaled overpotential

$$\vec{\nabla}^{*2}\varphi^* = \sinh\varphi^* \quad . \tag{2.19}$$

This implies that the scale for the charge density respectively the surface charge density are

$$\rho_c^* = \frac{ze}{\varepsilon\varepsilon_0\varkappa^2 kT}\rho_c \quad \text{and} \tag{2.20}$$

$$q^* = \frac{ze}{\varepsilon\varepsilon_0\varkappa kT}q \quad . \tag{2.21}$$

Since we consider a fluid at rest in a small layer, no inertia and gravity forces have to be taken into account. The equation of motion simplifies to a balance between pressure forces and electrodynamic forces. The scaling of the electrodynamic forces is given by Eqs. (2.17), (2.18) and (2.20). The pressure is scaled as in the classical gas theory by

$$p^* = \frac{p}{n_\infty kT} \quad . \tag{2.22}$$

This scaling is not surprising since the picture of the Boltzmann distribution for ion molecules bases on the treatment of fluid molecules as the molecules of an ideal gas. Using Eqs. (2.17), (2.18), (2.20) and (2.22) and the definition of $\varkappa^2$ the scaled equation of motion reads as

$$\vec{\nabla}^* p^* = -2\vec{\nabla}^*\varphi^* \quad . \tag{2.23}$$

In order to give some clear insights in the physics, we first treat free surfaces under the simplified linear approach of Debye-Hückel in their real physical dimensions. Then we will treat the complete non-linear problem. To simplify the mathematics we solve the analytical problem in the dimensionless way.

Chapter 3

Free Surfaces.

3.1 Debye-Hückel Linear Approach.

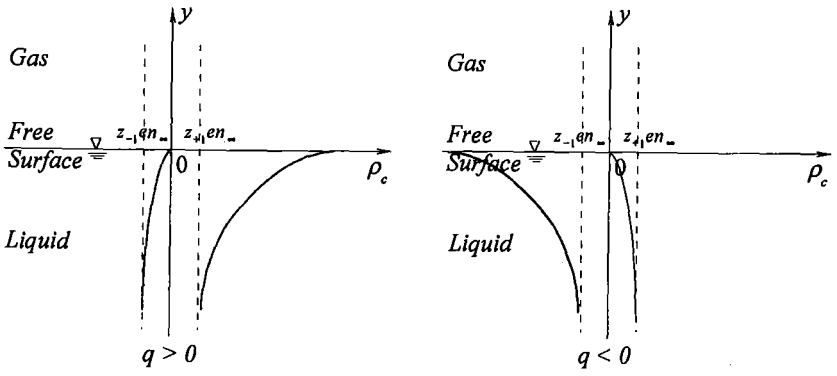

Figure 3.1: Plane, free surface: coordinate system.

Consider a plane, free surface of a liquid with coordinates as defined in Fig (3.1). The surface at position $y = 0$ is treated one-dimensionally. The density of the adjacent gas is neglected against ρ, so that it can be treated as with zero charge. We assume that the overpotential φ is much smaller than 25 mV, so that the Debye-Hückel approximation with charge density (2.5) can be applied. Under this approximation the Poisson-Boltzmann equation (2.8) can be linearized to

$$\frac{\partial^2 \varphi}{\partial y^2} = -\sum_i \frac{z_i e n_{i\infty}}{\varepsilon \varepsilon_0} \left(1 - \frac{e\, z_i\, \varphi}{kT}\right) \quad . \tag{3.1}$$

Using the condition of an electrically neutral bulk (2.3), Eq. (3.1) can be written as:

$$\frac{\partial^2 \varphi}{\partial y^2} = \varkappa^2 \varphi \quad , \tag{3.2}$$

with the Debye-Hückel parameter $\varkappa$ defined by Eq. (2.14). The general solution to Eq. (3.2) with integration constant A is

$$\varphi = A \exp(\varkappa y) \qquad \text{for } y < 0 \quad . \tag{3.3}$$

The constant A is determined from the boundary conditions

$$\varphi(y \to -\infty) = 0 \qquad \text{and} \qquad \frac{\partial \varphi}{\partial y}(y=0) = \frac{q}{\varepsilon\varepsilon_0} \quad , \tag{3.4}$$

and yields

$$A = \frac{q}{\varepsilon\varepsilon_0 \varkappa} \quad . \tag{3.5}$$

Ions and counter-ions in the microlayer form a capacitor of thickness $1/\varkappa$ and relative dielectric constant ε of the liquid. Its electrical energy has to be added to the surface energy γ_0 of the nanolayer to yield the total surface energy γ_L as:

$$\gamma_L = \gamma_0 + \frac{1}{2}\int_{-\infty}^{0} \rho_c \varphi dy + \frac{1}{2} q\varphi(0) \quad . \tag{3.6}$$

Substitution of Eqs. (2.5), (3.3) and (3.5) in Eq. (3.6) results after some algebra in the simple relation

$$\gamma_L = \gamma_0 + \frac{1}{4}\frac{q^2}{\varepsilon\varepsilon_0 \varkappa} \quad . \tag{3.7}$$

The surface energy (3.7) of the liquid is composed by the nanolayer energy and a positive microlayer energy, independently of the sign of the surface charge q. Since the surface energy of liquids is a well known, macroscopic liquid property, a closure relation either for the surface charge density q or for the surface energy γ_0 can be determined, if one of these properties has been determined experimentally. Since in reality the overpotential is larger than 25 mV, no linear Debye-Hückel approximation can be assumed and these relation has to be evaluated quantitatively in the non-linear approach.
A closer look on the stresses in the microlayer can ease the understanding of the EDL approach. Considering the liquid at rest and assuming that the pressure gradient and the Coulomb forces are dominating, Eq. (2.15) can be simplified to

$$\frac{dp}{dy} = -\rho_c \frac{d\varphi}{dy} \quad . \tag{3.8}$$

With the overpotential (3.3) with constant (3.5), and with the charge density (2.5), Eq. (3.8) yields for the pressure distribution in the liquid region:

$$p(y) = p_{-\infty} + \frac{q^2}{2\varepsilon\varepsilon_0}\exp(2\varkappa y) \qquad \text{for } y < 0 \quad , \tag{3.9}$$

where $p_{-\infty}$ is the pressure in the bulk of the fluid[1]. This positive pressure head in the EDL is certainly surprising, since the surface layer has a tensile surface stress. The surface forces become clearer if we look at the electrostatic stresses.

[1] At the surface, the charge density ρ_c jumps from $\rho_c(0-) = -\varkappa q$ to $\rho_c(0+) = (1-\varkappa)q$ because the charge density of the nanolayer is added to the charge density of the microlayer. Therefore the pressure at $y = 0$ jumps from $p(0-) = p_{-\infty} + \frac{1}{2}\frac{q^2}{\varepsilon\varepsilon_0}$ to $p(0+) = p_{-\infty} - \frac{1}{2}\frac{q^2}{\varepsilon\varepsilon_0}$.

According to Landau and Lifschitz (1973) the electrostatic Maxwell stress tensor σ_{ik}^{el} for an electric field $\vec{\mathbf{E}}$ is given by

$$\sigma_{ik}^{el} = \varepsilon\varepsilon_0 \left(\frac{E^2}{2}\delta_{ik} - E_i E_k \right) \quad . \tag{3.10}$$

In our case, with $\vec{\mathbf{E}} \parallel \vec{\mathbf{y}}$, the stress component parallel to the surface (in $\vec{\mathbf{x}}$-direction) is determined as

$$\sigma_{xx}^{el} = \frac{\varepsilon\varepsilon_0}{2} E_y^2 = \frac{q^2}{2\varepsilon\varepsilon_0} \exp(2\varkappa y) \quad . \tag{3.11}$$

The total surface tension σ, acting within the microlayer, can be integrated from this stress component as

$$\sigma = \int_{-\infty}^{0} \sigma_{xx}^{el}\, dy \quad . \tag{3.12}$$

Inserting Eq. (3.11) into Eq. (3.12) gives after integration

$$\sigma = \frac{1}{4} \frac{q^2}{\varepsilon\varepsilon_0 \varkappa} \quad . \tag{3.13}$$

In other words, the surface tension σ in Eq. (3.13) equals the surface energy γ_L of the microlayer, given by Eq. (3.7). Our model is consistent with the classical definition of the surface tension as the specific energy needed to enlarge the surface. Since σ is positive, independently of the sign of q, the resulting surface tension is always tensile.
On the other hand, Eq. (3.10) gives the stress component normal to the surface (in $\vec{\mathbf{y}}$-direction) as

$$\sigma_{yy}^{el} = -\frac{\varepsilon\varepsilon_0}{2} E_y^2 = -\frac{q^2}{2\varepsilon\varepsilon_0} \exp(2\varkappa y) \quad , \tag{3.14}$$

which can be integrated to $-\sigma$ over the total surface layer. Therefore, the resulting Maxwell stress tensor is anisotropic with two tensile components parallel to the surface, and a compressive component normal to the surface[2].
To illustrate the results, we plot the derived functions for free liquid surface in Fig. (3.2). We show for the case of water as liquid

- the overpotential φ, scaled with $q/(\varepsilon\varepsilon_0\varkappa)$
- the charge densities ρ_c, scaled with $q\varkappa$
- the pressure $p - p_{-\infty}$, scaled with $q^2/(\varepsilon\varepsilon_0)$, and
- the electrostatic stress component σ_{xx}^{el}, also scaled with $q^2/(\varepsilon\varepsilon_0)$
- the electrostatic stress component σ_{yy}^{el}, also scaled with $q^2/(\varepsilon\varepsilon_0)$

as a function of the dimensionless coordinate $\varkappa y$.

[2]Although the components of the resulting stress tensor $\overleftrightarrow{\Sigma} = \begin{bmatrix} \sigma_{xx}^{el} + p - p_\infty & 0 \\ 0 & \sigma_{yy}^{el} + p - p_\infty \end{bmatrix}$ induce a force, no force $\vec{\mathbf{F}}$ acting on the surface may exist, since the fluid has to remain at rest. Looking at $\vec{\mathbf{F}} = \int_{-\infty}^{0} \overleftrightarrow{\Sigma} \cdot d\vec{\mathbf{y}} = \vec{\mathbf{0}}$, the force $\vec{\mathbf{F}} \parallel \vec{\mathbf{y}}$ on the surface indeed vanishes.

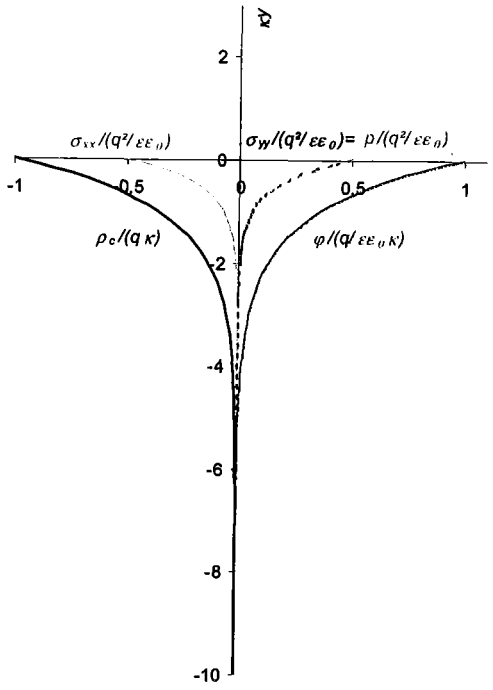

Figure 3.2: Scaled profiles of the overpotential, the charge density, the pressure and the electrostatic stress components. This case represents exemplary a water/air surface in which the overpotential is $< 25mV$.

3.2 Non-Linear Analytical Solution.

We consider the same free surface system as described under section 3.1 but concentrate on symmetrically polyvalent liquids. The density of the adjacent gas is neglected against ρ, and it is treated as with zero charge. The total charge density is related to the overpotential by Eq. (2.7). For this one-dimensional case, with the surface at position $y = 0$, and with the scaling as introduced at the end of section 2.4, Eq. (2.19) simplifies to

$$\frac{d^2\varphi^*}{dy^{*2}} = \sinh\varphi^* \quad . \tag{3.15}$$

By multiplying both sides of Eq. (3.15) with $d\varphi^*/dy^*$ this equation is equivalent to

$$\frac{1}{2}\frac{d}{dy^*}\left(\left(\frac{d\varphi^*}{dy^*}\right)^2\right) = \frac{d}{dy^*}(\cosh\varphi^*) \quad . \tag{3.16}$$

The boundary conditions for the electric overpotential are given by

$$\varphi^* \ (y^* \to -\infty) \ = \ 0 \quad , \tag{3.17}$$

$$\frac{d\varphi^*}{dy^*} (y^* \to -\infty) \ = \ 0 \quad \text{and} \tag{3.18}$$

$$\frac{d\varphi^*}{dy^*} (y^* = 0) \ = \ q^* \quad . \tag{3.19}$$

Integration of Eq. (3.16) from $-\infty$ till y^* leads to

$$\left(\frac{d\varphi^*}{dy^*}\right)^2 = 2\left(\cosh\varphi^* - 1\right) = 4\sinh^2\frac{\varphi^*}{2} \quad . \tag{3.20}$$

The boundary conditions (3.17 to 3.19) allow only solutions in which φ^* and $d\varphi^*/\,dy^*$ have the same sign, so that the square root of Eq. (3.20) has the only solution

$$\frac{d\varphi^*}{dy^*} = +2\sinh\frac{\varphi^*}{2} \quad . \tag{3.21}$$

Further integration results in

$$\ln\left(\tanh\frac{\varphi^*}{4}\right) = y^* + c \quad , \tag{3.22}$$

so that the solution for φ^* evaluates as

$$\varphi^*(y^*) = 4\,\text{arctanh}\left(A\exp y^*\right) \quad . \tag{3.23}$$

The constant of integration $A = \exp c$ is determined by boundary condition (3.19) as

$$\frac{d\varphi^*}{dy^*}(0) = 2\sinh\frac{\varphi^*(0)}{2} = q^* \quad , \tag{3.24}$$

so that

$$\varphi^*(0) = 2\,\text{arcsinh}\frac{q^*}{2} \quad , \tag{3.25}$$

and

$$A = \tanh\left(\frac{\varphi^*(0)}{4}\right) = \tanh\left(\frac{1}{2}\,\text{arcsinh}\frac{q^*}{2}\right) \quad . \tag{3.26}$$

Finally, the electric overpotential[3] can be written as

$$\varphi(y) = \frac{4kT}{ze}\,\text{arctanh}\left(A\exp(\varkappa y)\right) \quad , \tag{3.27}$$

or after using the logarithmic expression[4] for $\text{arctanh}\left(A\exp(\varkappa y)\right)$ as

$$\varphi\,(y) = \frac{2kT}{ze}\ln\left(\frac{1 + A\exp\left(\varkappa y\right)}{1 - A\exp\left(\varkappa y\right)}\right) \quad . \tag{3.28}$$

[3]Note that symmetrically to the positive solution for φ (by definition of the logarithmic function) also a negative solution $\varphi < 0$ is mathematically possible given by $\varphi = -\frac{4kT}{e}\,\text{arctanh}\left(\exp(\varkappa\,(y + c))\right)$.

[4]Taking the derivative of this logarithmic expression for φ and inserting the boundary condition for $d\varphi/\,dy$ at $y = 0$ results for A in the following expression: $A = \left(4en_\infty/\,\varkappa + \sqrt{\left(4en_\infty/\,\varkappa\right)^2 + 1}\right)^{-1}$.

Thereby, with use of the identity

$$\frac{2\varepsilon\varepsilon_0 \varkappa kT}{ze} = \frac{4zen_\infty}{\varkappa} \quad , \tag{3.29}$$

the surface overpotential $\varphi(0)$ can be expressed as :

$$\varphi(0) = \frac{2kT}{ze} \operatorname{arcsinh}\left(\frac{\varkappa}{4zen_\infty} q\right) \quad . \tag{3.30}$$

The expression (3.27) indicates that the overpotential φ decreases in the microlayer faster than an exponential decay with increasing distance y from the surface. For $A << 1$ the decay approaches the exponential solution[5].
Looking again to the electrical energy of the capacitor, formed by the ions and counter-ions in the microlayer and defined by Eq. (3.6), we get

$$\gamma_L = \gamma_0 + \frac{1}{2}\int_{-\infty}^{0} \rho_c \varphi dy + \frac{1}{2} q\varphi(0) \quad . \tag{3.31}$$

Substitution of the charge density (2.7) in Eq. (3.31) followed by integration by parts and then by substitution of the derivative of the overpotential (3.28) results in

$$\gamma_L = \gamma_0 + \frac{8n_\infty kT}{\varkappa} \frac{A^2}{1-A^2} \quad . \tag{3.32}$$

As A is always less than 1, the surface energy of the microlayer turns out to be always positive. Since the surface energy of liquids is a well known, macroscopic liquid property, a closure relation either for the surface charge density q or for the surface energy γ_0 can be determined, if one of these properties has been determined experimentally.
Analogously as under the linear approach of section 3.1 the stresses in the microlayer can be derived. With the charge density (2.7), Eq. (3.8) yields for the pressure distribution in the liquid region:

$$p(y) = p_{-\infty} + \frac{\varepsilon\varepsilon_0}{2}\int_{-\infty}^{y} d\left(\frac{d\varphi}{dy}\right)^2 \qquad \text{for } y < 0 \quad , \tag{3.33}$$

where $p_{-\infty}$ is the pressure in the bulk of the fluid. Substitution of the derivative of the overpotential (3.28) in Eq. (3.33) gives for the pressure

$$p(y) = p_{-\infty} + 16\, n_\infty kT \frac{A^2 \exp(2\varkappa y)}{(1 - A^2 \exp(2\varkappa y))^2} \qquad \text{for } y < 0 \quad . \tag{3.34}$$

[5]In the limit for $ze\varphi(0) << 4kT$ or $\frac{q}{\varepsilon\varepsilon_0\varkappa} << \frac{2kT}{ze}$ or $\frac{\varkappa^2}{4en_\infty} << 1$, the overpotential φ with constant A can be expressed by the simple exponential function with constant $\frac{q}{\varepsilon\varepsilon_0\varkappa}$. Since in this case $A << 1$ and $y < 0$, the expression $\ln(1 + A\exp(\varkappa y))$ can be linearised as $A\exp(\varkappa y)$. Analogously is $-\ln(1 - A\exp(\varkappa y)) \approx A\exp(\varkappa y)$. Under the same conditions, the constant A can be approximated by $\varphi(0)$ and $\varphi(0)$ by $\frac{2kT}{ze}\frac{\varkappa}{4en_\infty} = \frac{q}{\varepsilon\varepsilon_0\varkappa}$.

The mechanical surface forces acting within the microlayer are to be derived from the electrostatic stresses Eq. (3.10). Substituting the electric field in the microlayer $\vec{E} \parallel \vec{y}$, the stress component parallel to the surface (in $\vec{x}$-direction) is determined as

$$\sigma_{xx}^{el} = \frac{\varepsilon\varepsilon_0}{2} E_y^2 = 16\, n_\infty kT \frac{A^2 \exp(2\varkappa y)}{(1 - A^2 \exp(2\varkappa y))^2} \quad , \tag{3.35}$$

and the stress component normal to the surface (in $\vec{y}$-direction) as

$$\sigma_{yy}^{el} = -\frac{\varepsilon\varepsilon_0}{2} E_y^2 = -16\, n_\infty kT \frac{A^2 \exp(2\varkappa y)}{(1 - A^2 \exp(2\varkappa y))^2} \quad . \tag{3.36}$$

The electric part of the surface tension σ, acting within the microlayer, can be evaluated by integration of this stress component as

$$\sigma = \int_{-\infty}^{0} \sigma_{xx}^{el}\, dy \quad . \tag{3.37}$$

Inserting Eq. (3.35) into Eq. (3.37) gives after integration

$$\sigma = \frac{8\, n_\infty kT}{\varkappa} \frac{A^2}{1 - A^2} \quad . \tag{3.38}$$

Again the surface tension σ equals the electric energy of the microlayer given by Eq. (3.32), so that the electric energy of the microlayer is equal to the mechanical stretching energy in the tangential direction. Independently of the sign of q, the resulting surface tension remains always tensile. This confirms that the resulting Maxwell stress tensor is anisotropic with two tensile components parallel to the surface, and a compressive component normal to the surface.
For illustration we plot in Fig. (3.3)

- the overpotential φ, scaled with $kT/(ze)$,
- the charge densities[6] ρ_{c-} and ρ_{c+}, scaled with $n_\infty ze$,
- the pressure $p - p_{-\infty}$, scaled with $n_\infty kT$,
- the electrostatic stress component σ_{xx}^{el}, scaled with $n_\infty kT$, and
- the electrostatic stress component σ_{yy}^{el}, also scaled with $n_\infty kT$

as a function of the dimensionless coordinate $\varkappa y$.

[6]To give an idea of the behaviour of the positive and negative ions separately we have split up the charge density $\rho_c = \rho_{c+} + \rho_{c-}$.

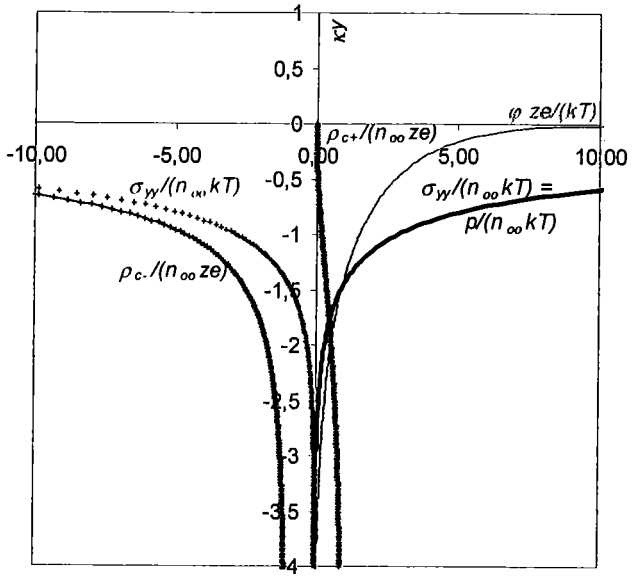

Figure 3.3: Scaled profiles of the overpotential, the charge densities, the pressure and the electrostatic stress components. This represents typically the behaviour of a Hg/air surface.

3.3 Evaluation of the Surface Parameters.

The surface charge density can be measured from the deflection of falling drops in an electric field. Polat, Polat and Chander (2000) performed such experiments with water droplets and determined a surface charge of less than $5\,10^{-8}$ C/m^2. Moreover Bailey (1988) stated that the surface charge density in electrolytic systems is of the order of $3\,10^{-10}$ C/m^2. The electric energy of the microlayer, based on this surface charge, is less than $8.5\,10^{-13}$ J/m^2. This contribution is negligibly small compared to the measured surface energy of pure water of 0.073 J/m^2 at 20°C. As a consequence, we assume the surface charge q zero and the surface energy of the nanolayer γ_0 equal to 0.073 J/m^2 at 20°C. Also for other aqueous solutions $q = 0$ is a fairly good approximation.

Levich (1962) reports on an a similar experiment by Frumkin and Bagotskaya (1948), in which mercury drops were deflected towards the cathode even if their surface overpotential was zero, which caused a small difference to their predictions. Our theory can explain this difference now. Since an uncharged droplet would have a surface overpotential $\varphi(0)$, according to Eq. (3.26), a surface charge density of $-q$ has to be added in order to get a zero surface overpotential. From these experimental results we determine the charge q to be positive and equal to approximately $5\ 10^{-6}$ C/cm^2. Since the EDL-theory to our knowledge has not yet been applied to liquid metals, the Debye length for liquid mercury is not known from literature. However, according to Adamson (1976) the initially positive charge of a mercury surface can be reduced by an applied potential. The maximum reduction is observed at -0.480 V, when the Lippmann's electrocapillary curve reaches a maximum interfacial tension. This compensation of the overpotential at the mercury surface with zero surface charge allows to conclude that the overpotential at the free surface of liquid

Fluid	Surface energy	Debye length	Surface Charge	Nanolayer Energy
H_2O	0.0727 N/m	966 nm	$5\,10^{-8}$ C/m^2	0.0727 N/m
Hg	0.476 N/m	65 nm	0.05 C/m^2	0.475 N/m
0.1M NaCl	0.0729 N/m	0.968 nm	$5\,10^{-8}$ C/m^2	0.0729 N/m

Table 3.1: Examples of the surface energy as macroscopic property, the Debye length and the surface charge as microscopic properties for some fluids at $20°C$.

Hg is about 0.480 V. With Eqs. (3.26) and (3.29) we estimate a Debye length of 65 nm for liquid mercury. The electric energy in the microlayer of liquid Hg with thickness $\varkappa^{-1} = 65$ nm due to the surface charge $q = 0.05$ C/m^2 is approximately $1.25\ 10^{-3}$ J/m^2. With the measured surface energy of Hg of 0.476 J/m^2 at 20°C, we can conclude that the microlayer of Hg does not include any significant surface energy again. Instead, most of the surface energy γ_0 is concentrated in the nanolayer, which amounts to 0.475 J/m^2 at 20°C.

Chapter 4

Interface of a Liquid at a Solid Wall.

4.1 Non-Linear Analytical Solution.

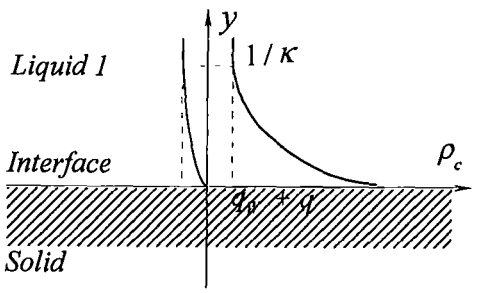

Figure 4.1: Liquid / solid interface: coordinate system.

In this section a liquid facing an electrically, non-conducting, plane wall is considered. The system is said to be in thermostatic equilibrium if it is in a configuration of minimum energy. In this wall with e.g. a crystalline structure mobile ions are not present. The crystal ions can only vibrate around there lattice positions. In the presence of some counter-ions of a liquid the crystal ions can only shift over their vibration distance. Therefore a fixed wall surface charge density q_W has to be taken into account. The surface charge density q and the surface energy γ_0 of the nanolayer are assumed to be still the same as for free surfaces. For the symmetrically polyvalent liquid on the wall, in the coordinate system as sketched in Fig. (4.1), a local overpotential φ is related to the total charge density of the liquid by Eq. (2.7), which simplifies to

$$\rho_c = -\varepsilon\varepsilon_0 \frac{d^2\varphi}{dy^2} \quad . \tag{4.1}$$

At the surface, the overpotential fulfills boundary condition (2.10) with the total charge density at the surface $q_W + q$ by

$$\frac{d\varphi}{dy}(0) = \frac{q + q_W}{\varepsilon\varepsilon_0} \quad . \tag{4.2}$$

As in section 3.2, the general solution for the overpotential φ can be given by

$$\varphi(y) = \frac{2kT}{ze} \ln\left(\frac{1 + A_S \exp(-\varkappa y)}{1 - A_S \exp(-\varkappa y)}\right) \qquad \text{if } y > 0, \tag{4.3}$$

with the constant of integration

$$A_S = \tanh\left(\frac{ze\varphi(0)}{4kT}\right) \quad . \tag{4.4}$$

The surface overpotential $\varphi(0)$ and so the constant of integration A_S are determined from the boundary condition (4.2), which leads after some algebra to a similar relation as Eq. (3.26), namely

$$\varphi(0) = \frac{2kT}{ze} \operatorname{arcsinh}\left(\frac{\varkappa}{4zen_\infty}(q + q_W)\right) \quad . \tag{4.5}$$

The surface energy of the liquid in contact with the solid $\gamma_L^{(S)}$ is different from that of a free surface. Like in Eq. (3.6) we determine it as

$$\gamma_L^{(S)} = \gamma_0 + \frac{1}{2}\int_0^\infty \rho_c \varphi \, dy + \frac{1}{2} q\varphi(0) \quad . \tag{4.6}$$

After inserting the charge density of the liquid in Eq. (4.6), performing integration by parts and substituting the overpotential's derivative, the liquid / solid interfacial surface energy $\gamma_L^{(S)}$ of the liquid is determined as

$$\gamma_L^{(S)} = \gamma_0 + \frac{8\, n_\infty kT}{\varkappa} \frac{A_S^2}{1 - A_S^2} - q_W \frac{kT}{ze} \operatorname{arcsinh}\left((q + q_W)\frac{\varkappa}{4zen_\infty}\right) \quad . \tag{4.7}$$

The interfacial surface energy of the liquid is composed by three terms. The first term includes the surface energy of the nanolayer, which we assume to be independent of the wall charge density. The second term is the electric energy of the capacitor formed by the wall charge density plus the charge density of the nanolayer as one plate, and by the microlayer as the other plate. The third term is the electric energy of the wall itself, which is not part of the liquid surface, and therefore negative.

Obviously, the liquid / solid interfacial surface energy $\gamma_L^{(S)}$ of a liquid is different from the surface energy γ_L of its free surface, Eq. (3.32). We can show in Eq. (4.7) that $\gamma_L^{(S)}$ must always be less than γ_L, independently of the sign of q and q_W. It is surprising, however, to see that $\gamma_L^{(S)}$ can even become negative. The latter case may not be interpreted as if the energy would be released if the liquid is separated from the wall. It can easily be shown that the total interfacial surface energy, including that of the wall surface charge density q_W, is always positive. This means that work will be required to separate the liquid from the wall.

The wall surface charge density q_W can hardly be measured. Instead, we will show how q_W can be derived from the static contact angle θ of a liquid droplet on a solid wall, as sketched in Fig. (4.2). We assume that the gas surrounding the droplet has a negligible charge density, so that we can treat it as electrically neutral. The static contact angle takes

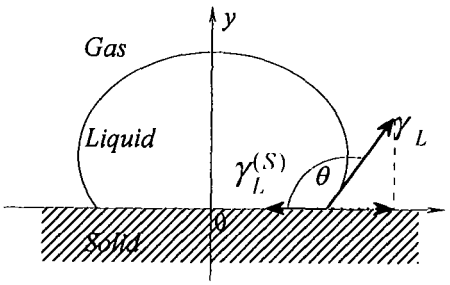

Figure 4.2: Model for a liquid droplet on a solid wall.

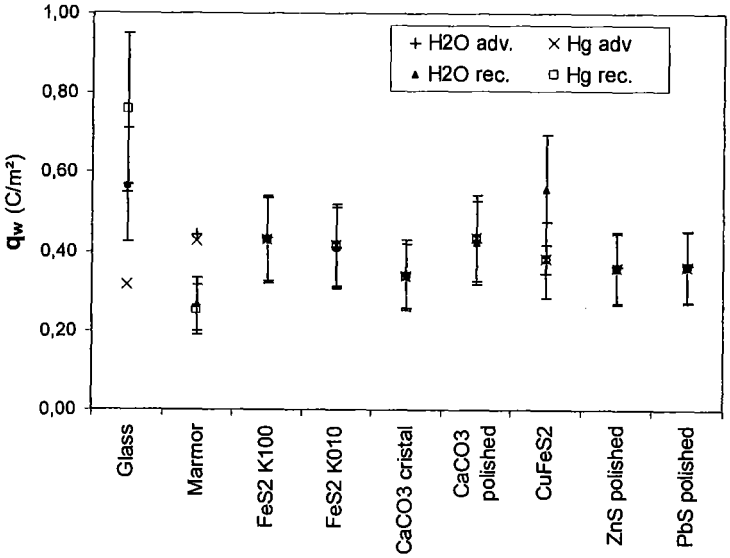

Figure 4.3: Comparison of the wall surface charge, determined by correlation (4.9) for H_2O and Hg with measured data for the advancing and receding contact angles from Landolt-Börnstein (1956).

a value, so that the total surface energy of the liquid, which is the free surface energy of the liquid droplet plus the surface energy of the droplet in contact with the solid, becomes a minimum. Using geometric constraints for a droplet of constant volume as in Fig. (4.2), the criterium of vanishing total free energy change leads to:

$$\gamma_L^{(S)} + \gamma_L \cos\theta = 0 \quad . \tag{4.8}$$

This equation is identical with the equation of Young (1805), under the assumption that the surface energy of the gas at the wall is zero. Inserting Eqs. (3.32) and (4.7) into Eq. (4.8) yields

$$\cos\theta = \frac{A^2/(1-A^2) - A_S^2/(1-A_S^2) + q_W \varkappa/(4zen_\infty) \operatorname{arctanh}(A_S)}{\gamma_0 \varkappa/(8n_\infty kT) + A^2/(1-A^2)} - 1 \quad . \tag{4.9}$$

4.2 Debye-Hückel Limit.

In the limit for $e\varphi(0) << 4kT$ or $\frac{q}{\varepsilon\varepsilon_0\varkappa} << \frac{2kT}{e}$ or $\frac{\varkappa^2}{4en_\infty} << 1$, the overpotential φ can as solution of the linearized Poisson-Boltzmann equation with boundary condition (4.2) be expressed by the simple exponential function

$$\varphi = \frac{q + q_W}{\varepsilon\varepsilon_0\varkappa} \exp(-\varkappa y) \qquad \text{if } y > 0 \quad . \tag{4.10}$$

The charge density of the liquid, which does not include the wall surface charge q_W at $y = 0$, is with Eqs. (2.5) and (4.10) determined by

$$\rho_c = \varkappa(q + q_W)\exp(-\varkappa y) \quad . \tag{4.11}$$

The surface energy of the liquid in contact with the solid $\gamma_L^{(S)}$ is like in section 4.1 determined by Eq. (4.6) with the overpotential (4.10) and charge density (4.11) and results in

$$\gamma_L^{(S)} = \gamma_0 + \frac{1}{4}\frac{q^2}{\varepsilon\varepsilon_0\varkappa}\left(1 - \frac{q_W^2}{q^2}\right) \quad . \tag{4.12}$$

Using the result of Eq. (3.7) this expression can also be written with the free surface energy γ_L as

$$\gamma_L^{(S)} = \gamma_L\left(1 - \frac{q_W^2}{4\varepsilon\varepsilon_0\varkappa\gamma_0 + q^2}\right) \quad . \tag{4.13}$$

The liquid / solid interfacial surface energy $\gamma_L^{(S)}$ of a liquid is in the linear case simply given by the surface energy γ_L of its free surface and a correction factor $1 - q_W^2/q^2$. It is clearly noticed that $\gamma_L^{(S)}$ must always be less than γ_L and becomes negative for $q_W > q$. Since in real cases of e.g. water droplets on a glass plate, no linear Debye-Hückel approximation is allowed, we determine the wall surface charge density q_W in the next section from measured static contact angles with the non-linear analytical solution.

4.3 Validation by Measurements of Static Contact Angles.

Relation (4.9) allows to determine iteratively the wall surface charge density q_W by means of the static contact angle and of the liquid properties. In order to check the validity of this equation, we take data of two liquids with significantly different contact angles, water and mercury, and determine the wall surface charge densities for different wall materials independently. With the exception of glass we get an excellent agreement of both data, as shown in Fig. (4.3). The data differ by less than 10%, which is small compared with the difference up to 27% between q_W derived from the advancing contact angle and q_W derived from the receding contact angle in similar cases. Loman and Zwikker (1934) investigated especially the contact angles of water and mercury on different stones. The wall surface charge densities calculated using Eq. (4.9), with the contact angles measured by Loman and Zwikker, are represented in Fig. (4.4). The same behavior is clearly present in both

profiles for q_W. Taking into account the inaccuracy of the Hg properties, the difference of 20% in average is not too bad. The almost constant offset in Fig. (4.4) is mainly due to the error on q and can be reduced by a better estimation of $\varkappa$ and q for liquid mercury. Since the water properties are better known, we will use, further in this paper, the wall surface charges derived from the contact angle of the water droplets.

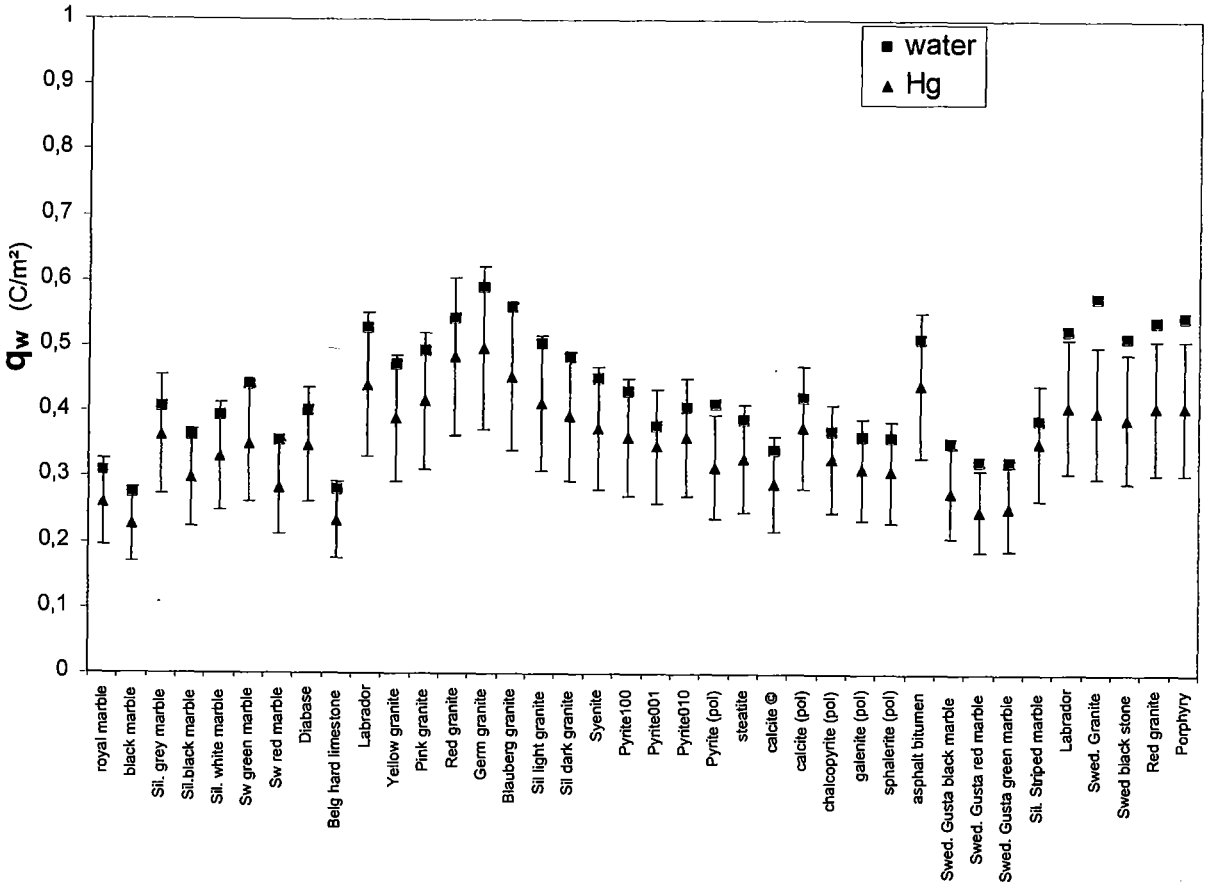

Figure 4.4: Comparison of the wall surface charge on different stone substrates, using the contact angle measurements of Loman and Zwikker (1934).

On the other hand, Eq. (4.9) allows us to predict the static contact angles of any liquid, which is within the scope of our model, once the static contact angle of water (or another liquid) with the individual wall material has been measured. As an example, the contact angle of aqueous solutions can be predicted as a function of the salt concentration, as shown in Fig. (4.5).

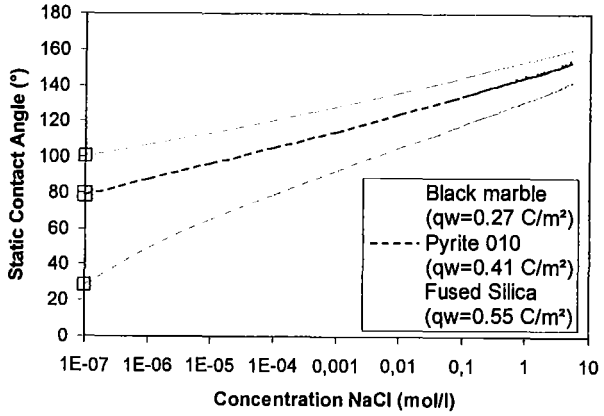

Figure 4.5: Contact angle for a NaCl solution on different walls as a function of the salt concentration. Thereby, q_W of the 3 substrates has been determined from the measured contact angle of H_2O.

Chapter 5

Interface of Two Immiscible Liquids.

5.1 Non-Linear Analytical Solution.

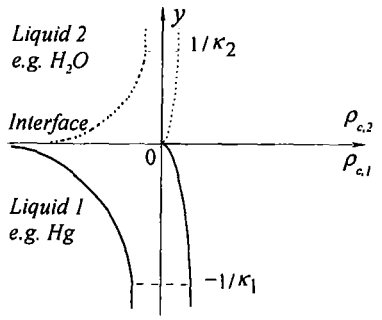

Figure 5.1: Plane liquid / liquid interface: coordinate system.

The planar interface of a less dense liquid 2 on top of a more dense liquid 1 in thermostatic equilibrium, with coordinates as defined in Fig. (5.1) is considered. The liquids 1 and 2 are characterized by ρ_{c1} (with z_1 and $n_{\infty 1}$), ε_1, $\varkappa_1$, γ_{01} respectively ρ_{c1} (with z_2 and $n_{\infty 2}$), ε_2, $\varkappa_2$, γ_{02} and are assumed to be symmetrically polyvalent. At the surface the mobile ions of liquid 1 and liquid 2 interact with each other. The Coulomb forces can influence strongly the ordering of those mobile ions performing a capacitor in both liquids with a surface charge density q_{12}, which differs from the free surface charge density. We concentrate on liquid 1, surrounded by liquid 2 with the nanolayer and microlayer of liquid 1. Performing the same procedure as in section 3 and scaling with the properties of liquid 1 leads to the Poisson-Boltzmann equation (3.15). To simplify the notation we introduce

$$\alpha = \frac{\varepsilon_2 \varkappa_2}{\varepsilon_1 \varkappa_1} \tag{5.1}$$

as ratio of the dielectric constant with the inverse of the Debye length for the less dense liquid to the more dense liquid and we present the results in their real physical dimensions. At the surface, the overpotential fulfills the boundary condition (2.10) with the surface

charge density q_{12} by

$$\frac{d\varphi}{dy}(0) = \frac{q_{12}}{\varepsilon_0 (1+\alpha)} \quad . \tag{5.2}$$

Note that with this boundary condition the total electroneutrality over both liquids

$$q_{12} - \varepsilon_1 \varepsilon_0 \int_{-\infty}^{0} \frac{\partial^2 \varphi}{\partial y^2} dy - \varepsilon_2 \varepsilon_0 \int_{0}^{+\infty} \frac{\partial^2 \varphi}{\partial y^2} dy = 0 \tag{5.3}$$

is fulfilled. As in section 3, the general solution for the overpotential φ can be given by

$$\varphi(y) = \frac{2kT}{z_1 e} \ln\left(\frac{1 + A_{12} \exp(\varkappa_1 y)}{1 - A_{12} \exp(\varkappa_1 y)}\right) \qquad \text{if } y < 0, \tag{5.4}$$

with the constant of integration

$$A_{12} = \tanh\left(\frac{z_1 e \varphi(0)}{4kT}\right) \quad . \tag{5.5}$$

The surface overpotential $\varphi(0)$ and so the constant of integration A_{12} are determined from the boundary condition (5.2), which leads again to the expression

$$\varphi(0) = \frac{2kT}{z_1 e} \operatorname{arcsinh}\left(\frac{\varkappa_1}{4 z_1 e n_{\infty 1}} \frac{1}{1+\alpha} q_{12}\right) \quad . \tag{5.6}$$

The interfacial surface energy of the liquid 1 in contact with liquid 2, noted by $\gamma_1^{(2)}$ is determined by Eq. (3.6) and results[1] in

$$\gamma_{L1}^{(L2)} = \gamma_{01} + \frac{8\, n_{\infty 1} kT}{\varkappa_1} \frac{A_{12}^2}{1 - A_{12}^2} - \frac{1}{1+\alpha} q_{12} \frac{kT}{z_1 e} \operatorname{arcsinh}\left(\frac{1}{1+\alpha} q_{12} \frac{\varkappa_1}{4 z_1 e n_{\infty 1}}\right) \quad . \tag{5.7}$$

The threefold composition of the interfacial surface energy $\gamma_{L1}^{(L2)}$ again appears with: (1) the surface energy of the nanolayer of liquid 1, (2) the electric energy of the capacitor between the nanolayer (which has electrically been modified by the influence of liquid 2) at one side and the microlayer of liquid 1 on the other side, and (3) the electric energy of the nanolayer itself which may not be counted in double by (1) and (2).
This interfacial surface energy $\gamma_{L1}^{(L2)}$ of liquid 1 in contact with liquid 2 can also be expressed in terms of the free surface energy of liquid 1. Substituting Eq. (3.32) into Eq. (5.7) leads to

$$\gamma_{L1}^{(L2)} = \gamma_{L1} - \frac{1}{1+\alpha} \frac{q_{12}}{2} \varphi(0) - \frac{8\, n_{\infty 1} kT}{\varkappa_1} \frac{A_{12}^2 - A_1^2}{(1 - A_{12}^2)(1 - A_1^2)} \quad . \tag{5.8}$$

In this Eq. (5.8) A_{12} is normally larger than A_1. Therefore this relation between $\gamma_1^{(2)}$ and γ_1 expresses that the surface energy of a liquid is reduced if it is surrounded by another liquid.

[1] after performing integration by parts and substituting the overpotential's derivative

5.2 Debye-Hückel Limit.

In the limit for $e\varphi(0) << 4kT$ or $q_{12}/(\varepsilon_1\varepsilon_0\varkappa_1 + \varepsilon_2\varepsilon_0\varkappa_2) << 2kT/e$, the linearized Poisson-Boltzmann equation with boundary condition (5.2) yields

$$\varphi = \frac{q_{12}}{\varepsilon_1\varepsilon_0\varkappa_1 + \varepsilon_2\varepsilon_0\varkappa_2} \exp(\varkappa_1 y) \qquad \text{if } y < 0 \quad . \tag{5.9}$$

The charge density of liquid 1 is with Eqs. (2.5) and (5.9) determined by

$$\rho_c = \frac{\varepsilon_1\varkappa_1^2 q_{12}}{\varepsilon_1\varkappa_1 + \varepsilon_2\varkappa_2} \exp(\varkappa_1 y) \quad . \tag{5.10}$$

The surface energy $\gamma_{L1}^{(L2)}$ of liquid 1 surrounded by liquid 2 is like in section 5.1 determined by Eq. (3.6) with the overpotential (5.9) and charge density (5.10) and results in

$$\gamma_{L1}^{(L2)} = \gamma_{01} + \frac{q_{12}^2(1+2\alpha)}{4\varepsilon_1\varepsilon_0\varkappa_1(1+\alpha)^2} \quad . \tag{5.11}$$

Using the result of Eq. (3.7) this expression can also be written with the free surface energy γ_{L1} as

$$\gamma_{L1}^{(L2)} = \gamma_{L1} - \frac{q_1^2(1+\alpha)^2 - q_{12}^2(1+2\alpha)}{4\varepsilon_1\varepsilon_0\varkappa_1(1+\alpha)^2} \quad . \tag{5.12}$$

For the quantitative validation in the following section the non-linear solution has to be taken because of the higher order of magnitude of q_{12} against q_1 in the case of e.g. water surrounded by Hg.

5.3 Validation for H_2O / Hg Surface.

It is not evident to determine the value of the surface charge at the interface of 2 immiscible liquids. For the case of water solutions and Hg it was possible to derive the magnitude of q_{12} from contact angle measurements reported by Landolt-Börnstein (1956). The contact angle of a 0.1 N H_2SO_4 solution on a liquid mercury layer has been measured by Möller (1908) as 85°. With the procedure of section 4.3 this contact angle yields a wall surface charge density of $q_W = 0.816\ C/m^2$. This q_W is also valid for the case of a water droplet on the same mercury layer, because water and aqueous solutions almost have the same surface charge density $q = 5.10^{-8}\ C/m^2$.
Comparing $q + q_W$ and q_{12} with $q_W = 0.816\ C/m^2$ and $q = 5.10^{-8}\ C/m^2$ yields the value $q_{12} = 0.816\,C/m^2$. The ratio α for this case of mercury / water is 0.185.
On the other hand Dunken (1940).measured the interfacial surface tension for mercury droplets in water and stated that the surface tension of mercury (in an inert gas atmosphere) $\gamma_{Hg} = 0.4859\,J/m^2$ was reduced to $\gamma_{Hg}^{(H2O)} = 0.3851\,J/m^2$ if the mercury was surrounded by water. For this case with $\alpha = 0.185$ and $q_{12} = 0.816\,C/m^2$ expression (5.8) can be validated. The second term of Eq. (5.8) evaluates as $0.118\,J/m^2$ and the third term as $0.00975\,J/m^2$. Therefore we calculate a reduction of $0.128\,J/m^2$ whereas the experimental data indicates a reduction of $0.101\,J/m^2$. This is a reasonable agreement (with only 5.6% difference) taking into account the measurement errors and the inaccuracy of the liquid properties.

Chapter 6

Liquid Flow in a Microchannel.

6.1 Linearized Approach.

6.1.1 Electro-Osmose by an Externally Applied Axial Electric Field.

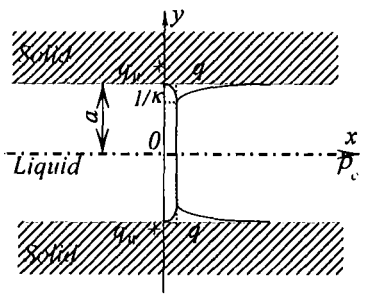

Figure 6.1: Model for a liquid flow through a solid microchannel.

The Poisseuille flow of a symmetrically polyvalent liquid (valence z) through a planar microchannel with gap width $2a$ and with electrically isolated and isothermal, solid walls is considered two-dimensionally[1] with coordinates (x, y), as sketched in Fig. (6.1). Gravity forces are neglected to simplify the analysis. The flow with velocity $\vec{\mathbf{w}}\,(u, v)$ is assumed to be fully developed, so that steady state flow conditions with a constant pressure drop Δp over a flow length l in the $\vec{\mathbf{x}}$-direction is established. Near the solid / liquid interface the electric double layer induces again a local electric overpotential φ. Moreover, we add a linear macroscopic potential Φ, which plays an important role for our solution, as will be shown further below. Since the thickness of the microlayer is much smaller than any macroscopic characteristic length scale, the macroscopic potential Φ can be assumed not to vary across the microlayer. We apply as macroscopic potential and pressure fields over

[1]The derivations in this section are also valid for a cylindrical capillary with cylindrical coordinates (r, z).

the considered flow length:

$$\frac{\partial \Phi}{\partial x} = -E_0 \quad \text{with} \quad \frac{\partial \Phi}{\partial y} = 0 \quad \Phi(x=0) = 0 \quad \text{and} \tag{6.1}$$

$$\frac{\partial p}{\partial x} = -\frac{\Delta p}{l} \quad . \tag{6.2}$$

As the flow is symmetric at $y = 0$, we get the following boundary conditions at the midplane:

$$\frac{\partial \varphi}{\partial y}(y=0) = 0 \quad , \quad \frac{\partial p}{\partial y}(y=0) = 0 \quad \text{and} \quad \frac{\partial u}{\partial y}(y=0) = 0 \quad . \tag{6.3}$$

Like in the classical fluid dynamics, we use no-slip boundary conditions for the velocity at the walls:

$$u(y=a) = u(y=-a) = 0 \quad . \tag{6.4}$$

The boundary conditions for the local overpotential in the microlayer at the solid / liquid surface are analogously as in Eq. (4.2) given by

$$\frac{\partial \varphi}{\partial y}(y=a) = \frac{q+q_W}{\varepsilon\varepsilon_0} \quad \text{and} \quad \frac{\partial \varphi}{\partial y}(y=-a) = \frac{q+q_W}{\varepsilon\varepsilon_0} \quad . \tag{6.5}$$

These conditions differ fundamentally from those in the analyses of the flow through a microchannel by Mala et al. (1996) or earlier by Rice and Whitehead (1965). They applied a Dirichlet boundary condition with constant overpotential at the walls instead of these Neumann boundary conditions (6.5).
To ease the physical understanding by simplifying the mathematics we first discuss the linearized problem under the Debye-Hückel approximation for small potentials $\varphi < kT/ze$. In the next section the complete problem with the non-linear analytical solution without any restriction to the potential will be treated.
The total potential $\varphi + \Phi$ has to fulfill the linearized Poisson-Boltzmann equation

$$\frac{\partial^2}{\partial x^2}(\varphi(y) + \Phi(x)) + \frac{\partial^2}{\partial y^2}(\varphi(y) + \Phi(x)) = \varkappa^2 \varphi \quad , \tag{6.6}$$

but since φ and Φ act on different length scales, Eq. (6.6) leads to the known Poisson-Boltzmann equation for the overpotential φ. which is given by Eq. (3.2). The general solution for the overpotential, fulfilling the symmetry conditions 6.3 reads:

$$\varphi = 2A\cosh(\varkappa y) \quad , \tag{6.7}$$

with the constant of integration A. This constant is determined by the boundary conditions (6.5) as

$$A = \frac{q+q_W}{2\varepsilon\varepsilon_0 \varkappa \sinh \varkappa a} \quad . \tag{6.8}$$

The total electric potential is because of the length scale separation given by the sum of the local overpotential $\varphi(x)$ plus the applied macroscopic potential $\Phi(y)$. This results in

$$\varphi + \Phi = \frac{q+q_W}{\varepsilon\varepsilon_0 \varkappa \sinh \varkappa a}\cosh(\varkappa y) - E_0 x \quad . \tag{6.9}$$

For a two-dimensional developed flow, under the assumption that gravity forces are negligible compared with the pressure gradient and with the Coulomb forces, the extended Navier-Stokes equation (2.15) can be simplified to

$$-\frac{\partial p}{\partial x}+\rho\nu\frac{\partial^2 u}{\partial y^2}-\rho_c\frac{\partial(\varphi+\Phi)}{\partial x} = 0 \quad , \tag{6.10}$$

$$-\frac{\partial p}{\partial y}-\rho_c\frac{\partial(\varphi+\Phi)}{\partial y} = 0 \quad . \tag{6.11}$$

The velocity profile $u(y)$ can be determined by two successive integrations of Eq. (6.10), taking into account the boundary conditions (6.3) and (6.4). This results in

$$u=\frac{1}{2}\frac{\Delta p}{\rho\nu l}\left(a^2-y^2\right)-\frac{E_0}{\rho\nu\varkappa}\left(q+q_W\right)\frac{\cosh\varkappa a-\cosh\varkappa y}{\sinh\varkappa a} \quad . \tag{6.12}$$

The velocity profile given by Eq. (6.12) is influenced by the gradient of the overpotential in the vicinity of the walls.
As in classical fluid dynamics for a pipe flow we scale the length by the pipe diameter, the velocity by

$$y^*=\frac{y}{a} \quad , \tag{6.13}$$

the velocity by

$$u^*=\frac{u}{a^2\Delta p/\left(2\rho\nu l\right)} \quad , \tag{6.14}$$

and the overpotential by

$$\varphi^*=\frac{\varphi}{\left(q+q_W\right)/\left(\varepsilon\varepsilon_0\varkappa\sinh\left(\varkappa a\right)\right)} \quad , \tag{6.15}$$

We define the characteristic number N_E as a ratio of electric to hydraulic forces

$$N_E=\frac{l(q+q_W)}{\varkappa a^2}\frac{E_0}{\Delta p} \quad , \tag{6.16}$$

and $N_\varkappa$ as a ratio of length scales

$$N_\varkappa=\varkappa a \quad . \tag{6.17}$$

The result (6.12) can with the definitions (6.16) and (6.17) be expressed in dimensionless way as

$$u^*=\left(1-y^{*2}\right)-2N_E\left(\cosh N_\varkappa-\cosh N_\varkappa y^*\right) \quad . \tag{6.18}$$

This solution satisfies no-slip at the wall and accounts for electric effects in the microlayer. We see that the velocity at position y^* is given by the superposition of the parabolic Poisseuille profile $(1-y^{*2})$ and a term $2N_E\left(\varphi^*\left(y^*\right)-\varphi^*\left(1\right)\right)$ due to the difference between the local overpotential and the overpotential at the wall surface. For $N_E>0$ the flow is driven by the pressure gradient and the electric field in the same direction (electrostatic pump). For $N_E<0$ the electric forces oppose the pressure driven fluid motion (electrostatic brake).

Averaging the velocity $u^*(y^*)$ over a whole cross section yields the mean velocity $\bar{u}^*$ in the microchannel, defined as

$$\bar{u}^* = \int_0^1 u^* \, dy^* \quad . \tag{6.19}$$

After substitution of Eq. (6.18) in Eq. (6.19), the scaled mean velocity results in

$$\bar{u}^* = \frac{2}{3} + 2N_E \left(\frac{1}{N_\varkappa} - \coth N_\varkappa \right) \quad . \tag{6.20}$$

For a channel with depth b the mean velocity, given by

$$\bar{u} = \frac{\Delta p a^2}{3\rho\nu l} \left(1 + 3N_E \frac{(1 - N_\varkappa \coth N_\varkappa)}{N_\varkappa} \right) \quad . \tag{6.21}$$

gives a mass flow $\dot{m} = 2ab\rho\bar{u}$ caused by an external pressure difference and an applied electric field, given by

$$\dot{m} = \frac{2}{3} \frac{a^3 b \Delta p}{\nu l} \left(1 + 3N_E \frac{(1 - N_\varkappa \coth N_\varkappa)}{N_\varkappa} \right) \quad . \tag{6.22}$$

Also the mean velocity and mass flow are influenced by the gradient of the overpotential. In the case of vanishing pressure drop the fluid can be driven by the electric field of strength E_0. This corresponds to an electro-osmotic flow with a speed to electric field ratio

$$\mu_{eo} = \frac{\bar{u}}{E_0} \tag{6.23}$$

$$= \frac{2\,(q + q_W)}{\varkappa\rho\nu} \left(\frac{1 - N_\varkappa \coth N_\varkappa}{N_\varkappa} \right) \quad . \tag{6.24}$$

This ratio is called the electro-osmotic mobility of the liquid. Under the non-linear approach we evaluate this electro-osmotic mobility of the liquid for real cases, to compare it with experimental findings.

6.1.2 Pressure Drop by the Self-Induced Axial Electric Field.

Near the wall a charge density distribution is established by the charged ions of the liquid, which are advected with the flow and which induce an electric current. The velocity profile (6.12) of the liquid, together with the charge density as given by Eq. (6.34), determines this streaming current I_s in the $\vec{x}$-direction as

$$I_s = \int_{-a}^{a} u \, \rho_c \, dy = 0 \quad . \tag{6.25}$$

Combining Eqs. (6.25), (6.12), (2.5) and (6.9) yields after some algebra

$$I_s = \frac{2\Delta p}{\rho\nu l} \frac{q + q_W}{\varkappa^2} (1 - \varkappa a \coth \varkappa a) + \frac{E_0 (q + q_W)^2}{\rho\nu\varkappa} \left(\coth \varkappa a - \frac{\varkappa a}{\sinh^2 \varkappa a} \right) \quad . \tag{6.26}$$

On the other hand, the electric field of strength E_0 causes also a current I_e in the $\vec{x}$-direction in the fluid. If we assume the electrical conductivity λ of the fluid to be constant, we simply get this conducting current as:

$$I_e = 2a\,\lambda\,E_0 \quad . \tag{6.27}$$

In this case that no external potential is applied, and if the walls of the microchannel are non-conducting, a potential is built up by the streaming current. Then I_e will act in the opposite direction of I_s. Under equilibrium conditions, both currents compensate each other:

$$I_e + I_s = 0 \quad . \tag{6.28}$$

This condition (6.28) provides the electro-neutrality along the microchannel at any cross section $x \neq 0$. Eq. (6.28) allows us to determine the strength E_0 of the electric field by the relation

$$E_0 = \frac{-2\Delta p\,(q+q_W)\,(1-\varkappa a\coth\varkappa a)}{l\varkappa\left(2\varkappa a\lambda\rho\nu+(q+q_W)^2\left(\coth\varkappa a-\varkappa a\sinh^{-2}\varkappa a\right)\right)} \quad . \tag{6.29}$$

Using the scaling proposed under Eqs. (6.13), (6.15), (6.16) and (6.17) and introducing the dimensionless number N_P, which includes the liquid and wall property data as

$$N_P = \frac{\lambda\rho\nu}{(q+q_W)^2} \tag{6.30}$$

Eq. (6.29) reads in dimensionless form

$$N_E = \frac{\coth N_\varkappa - 1/N_\varkappa}{N_p + \coth N_\varkappa/N_\varkappa - 1/\left(2\sinh^2 N_\varkappa\right)} \quad . \tag{6.31}$$

Since N_E increases with decreasing $N_\varkappa$, we can conclude that the electric field in the microlayer is enhancing with decreasing gap width.
For illustration we plot in Figs. (6.2) and (6.3):

- the overpotential $\varphi^*(y^*)$ at $x = 0$, and
- the velocity profile $u^*(y^*)$

  over the channel cross section for a theoretical parameter $N_p = 5\,10^{-6}$ and the parameter $N_\varkappa = 1, ..., 100$. The velocity profile shows a flow reversal due to the electric field. This explains also an enhanced pressure drop over the microchannel.

The pressure drop in many fluid dynamic applications is related to the inertial pressure drop. Introducing the Reynolds number of the channel $\mathrm{Re} = 2a\bar{u}/\nu$, Eq. (6.21) can be written in a dimensionless form we are used from classical fluid dynamics as

$$\frac{\Delta p}{\frac{\varrho}{2}\bar{u}^2} = \frac{24}{\mathrm{Re}}\frac{l}{2a}\left(1-3\frac{\left(1-N_\varkappa\coth N_\varkappa\right)^2}{N_p+\coth N_\varkappa/N_\varkappa-1/\left(2\sinh^2 N_\varkappa\right)}\right)^{-1} \quad . \tag{6.32}$$

The last factor in this result (6.58) for the pressure drop over the microchannel can be interpreted as a correction factor compared with that predicted by the Poisseuille flow theory. We evaluate this pressure drop correction factor for the non-linear analytical solution, since in real cases (e.g. water through a glass channel) the condition for the Debye-Hückel approximation is not fulfilled.

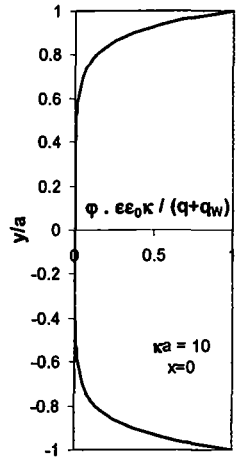

Figure 6.2: Potential at cross section $x = 0$, for a microchannel with size $\varkappa a = 10$.

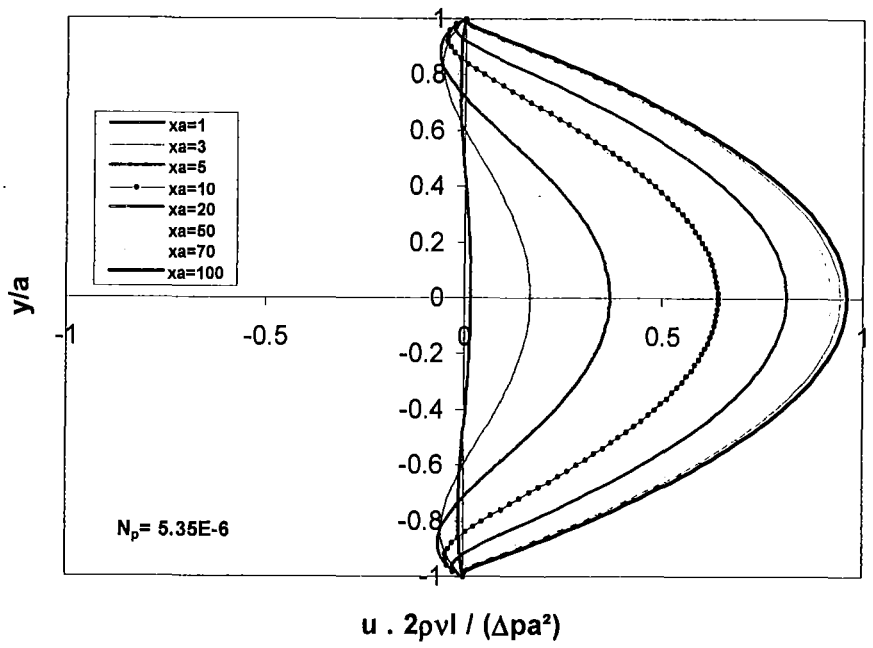

Figure 6.3: Velocity profile in microchannels for different sizes $\varkappa a$ for electrically isolated walls, without externally applied electric field but with a self-induced small electric potential $\varphi < kT/ze$.

6.2 Non-Linear Analytical Solution.

6.2.1 Electro-Osmose by an Externally Applied Axial Electric Field.

Analogously in section 6.1 we consider here the flow of a symmetrically polyvalent liquid (valence z) through a planar microchannel with gap width $2a$ and with isolated walls in

two dimensions, as represented in Fig. (6.1). We apply the same macroscopic potential and pressure fields as defined under Eqs. (6.1) and (6.2). Additionally the same assumptions and boundary conditions (6.3), (6.4) and (6.5) are applied for the flow, which is under this non-linear approach restricted to monovalent liquids.
The total potential $\varphi + \Phi$ has to fulfill the nonlinear Poisson equation

$$\frac{\partial^2}{\partial x^2}\left(\varphi(y) + \Phi(x)\right) + \frac{\partial^2}{\partial y^2}\left(\varphi(y) + \Phi(x)\right) = -\frac{\rho_c(y)}{\varepsilon\varepsilon_0} \quad , \tag{6.33}$$

but since φ and Φ act again on different length scales, Eq. (6.33) leads to the following Poisson-Boltzmann equation for the overpotential

$$\frac{\partial^2}{\partial y^2}\left(\varphi(y)\right) = -\frac{\rho_c(y)}{\varepsilon\varepsilon_0} \quad . \tag{6.34}$$

The general solution for the local overpotential at a single wall is equal to Eq. (4.3) with the constant of integration (4.4) with (4.5). If the gap width is large compared with the EDL thickness, the solutions in both layers decouple and we can solve them separately. Later we superpose the solutions for the two single layers to get an approximation for the flow in the microchannel. With U and L being the subscripts for the upper and lower wall, we get the overpotential functions

$$\varphi_U(y) = \frac{2kT}{ze}\ln\left(\frac{1 + A_S\exp\left(-\varkappa(a-y)\right)}{1 - A_S\exp\left(-\varkappa(a-y)\right)}\right) \qquad \text{for } y \le a \quad , \tag{6.35}$$

$$\varphi_L(y) = \frac{2kT}{ze}\ln\left(\frac{1 + A_S\exp\left(-\varkappa(a+y)\right)}{1 - A_S\exp\left(-\varkappa(a+y)\right)}\right) \qquad \text{for } y > -a \quad . \tag{6.36}$$

Thereby the function $|\varphi_U(y)|$ falls down with decreasing y from its maximum at $y = a$ towards a negligibly small value at $y = 0$. Analogously the function $|\varphi_L(y)|$ also falls down with increasing y from its maximum at $y = -a$ towards a negligibly small value at $y = 0$, so that superposition can be accepted. Superposing both functions in the common domain $[-a, a]$ yields then a smooth, symmetric solution $\varphi = \varphi_U + \varphi_L$, which is written as

$$\varphi(y) = \frac{2kT}{ze}\ln\left(\frac{1 + A_S\exp\left(-\varkappa a\right)\left(\exp\left(\varkappa y\right) + \exp\left(-\varkappa y\right)\right) + A_S^2\exp\left(-2\varkappa a\right)}{1 - A_S\exp\left(-\varkappa a\right)\left(\exp\left(\varkappa y\right) + \exp\left(-\varkappa y\right)\right) + A_S^2\exp\left(-2\varkappa a\right)}\right) \quad . \tag{6.37}$$

Introducing the constant

$$A_C = \frac{2A_S\exp\left(-\varkappa a\right)}{1 + A_S^2\exp\left(-2\varkappa a\right)}\cosh\left(\varkappa a\right) \tag{6.38}$$

simplifies the local overpotential $\varphi(y)$ as

$$\varphi(y) = \frac{2kT}{ze}\ln\left(\frac{1 + A_C\cosh\left(\varkappa y\right)/\cosh\left(\varkappa a\right)}{1 - A_C\cosh\left(\varkappa y\right)/\cosh\left(\varkappa a\right)}\right) \tag{6.39}$$

$$= \frac{4kT}{ze}\operatorname{arctanh}\left(A_C\cosh\left(\varkappa y\right)/\cosh\left(\varkappa a\right)\right) \quad . \tag{6.40}$$

The constant A_C,

$$A_C = \tanh\left(\frac{ze\varphi(a)}{4kT}\right) \quad , \tag{6.41}$$

is determined by the boundary condition (6.5) as

$$\frac{\partial\varphi}{\partial y}(y=\pm a) = \frac{4kT}{ze}\frac{\varkappa A_C \tanh(\varkappa a)}{1-A_C^2} = \frac{q+q_W}{\varepsilon\varepsilon_0} \quad . \tag{6.42}$$

Substituting Eq. (6.41) into Eq. (6.42) yields the local overpotential at the surfaces

$$\varphi(\pm a) = \frac{2kT}{ze}\operatorname{arcsinh}\left(\frac{q+q_W}{\varepsilon\varepsilon_0\varkappa}\frac{ze}{2kT}\coth(\varkappa a)\right) \quad . \tag{6.43}$$

The total electric potential is because of the length scale separation given by the sum of the local overpotential $\varphi(x)$ plus the applied macroscopic potential $\Phi(y)$. This results in

$$\varphi + \Phi = \frac{4kT}{ze}\operatorname{arctanh}\left(A_C\cosh(\varkappa y)/\cosh(\varkappa a)\right) - E_0 x \quad , \tag{6.44}$$

with the integration constant A_C determined by Eq. (6.42). Under the Debye-Hückel approximation in the limit for $A_C \approx \frac{q+q_W}{\varepsilon\varepsilon_0\varkappa}\frac{ze}{4kT}\coth(\varkappa a) << 1$, the total electric potential simplifies to Eq. (6.9).
The velocity profile $u(y)$ can be determined by two successive integrations of Eq. (6.10) from 0 to y, respectively from $-a$ till y, taking into account the expression for the charge density of Eq. (6.34) and the boundary conditions (6.3) and (6.4). With the constant (6.41) this results in

$$u(y) = \frac{1}{2}\frac{\Delta p}{\rho\nu l}\left(a^2-y^2\right) + \frac{\varepsilon\varepsilon_0 E}{\rho\nu}\frac{2kT}{ze}\ln\left(\frac{1+A_C\cosh(\varkappa y)/\cosh(\varkappa a)}{1-A_C\cosh(\varkappa y)/\cosh(\varkappa a)}\cdot\frac{1-A_C}{1+A_C}\right) \quad . \tag{6.45}$$

We use the scaling of the overpotential as defined in section 2.4 by Eq. (2.17) and we introduce the same geometric length scale and velocity scale as defined in section 6.1.1 by Eqs. (6.13) and (6.14) and the same dimensionless parameter $N_\varkappa$ defined by Eq. (6.17). Here the dimensionless number N_E again as a ratio of electric to hydraulic forces is defined by

$$N_E = \frac{8zen_\infty l}{(\varkappa a)^2}\frac{E_0}{\Delta p} \quad , \tag{6.46}$$

so that the result (6.12) can be represented in dimensionless way by

$$u^*(y^*) = \left(1-y^{*2}\right) + N_E\left(\ln\left(\frac{1+A_C\cosh(N_\varkappa y^*)/\cosh N_\varkappa}{1-A_C\cosh(N_\varkappa y^*)/\cosh N_\varkappa}\right) - \ln\frac{1+A_C}{1-A_C}\right) \quad . \tag{6.47}$$

Thereby the velocity at position y^* is again given by the superposition of the parabolic Poisseuille profile $(1-y^{*2})$ and a term $2N_E\left(\varphi^*(y^*)-\varphi^*(1)\right)$ due to the difference between the local overpotential and the overpotential at the wall surface. Results for the velocity are shown in Fig. (6.4) with exemplary both cases of an electrostatic pump for $N_E > 0$ and of an electrostatic brake for $N_E < 0$.

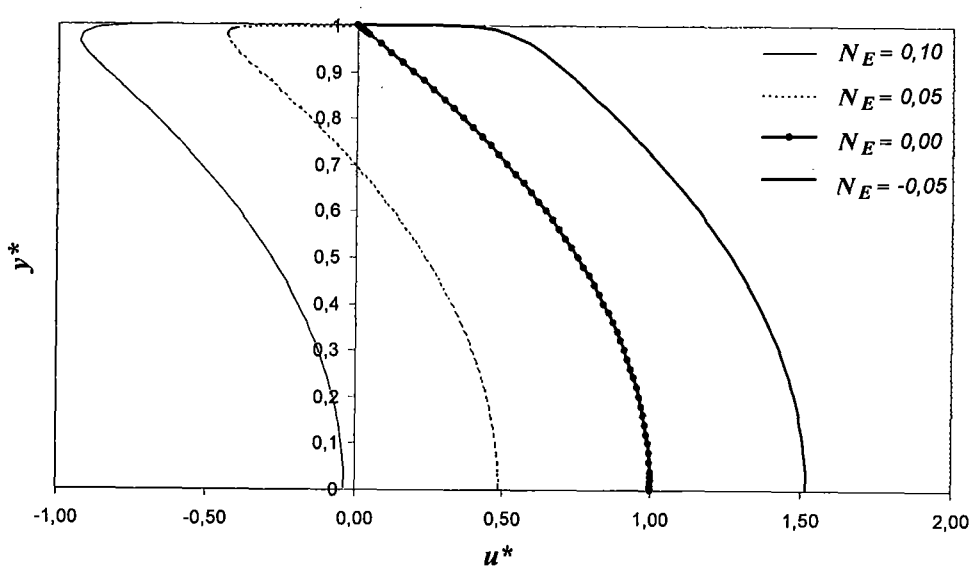

Figure 6.4: Effect of the ratio of electric to hydraulic forces on the velocity profile of a water flow throug a micro channel of size $N_\varkappa = 50$. In this case the constant $1 - A_C$ reaches $7\,10^{-5}$. The characteristic number N_E is defined by Eq. (6.46).

Substitution of Eq. (6.47) with constant (6.41) in Eq. (6.19) yields for the mean velocity

$$\bar{u}^* = \frac{2}{3} + 2N_E \int_0^1 \varphi^*\, dy^* - 2N_E\varphi^*(1) \quad . \tag{6.48}$$

To integrate the overpotential, the sum of the lower and upper potentials has been split-up in four integrals, which has been worked out with the help of Mathematica (Version by Wolfram (1996)). Using the Dilogarithm or Spence's Integral, defined by Abramowitz and Segun (1968) as

$$\mathrm{Li2}[x] = -\int_1^x \frac{\ln t}{t-1}\, dt = \sum_{k=1}^{\infty} \frac{(-1)^k (x-1)^k}{k^2} \qquad \text{for } 0 \le x \le 2, \tag{6.49}$$

the integral of the overpotential in Eq. (6.48) can be expressed by

$$\int_0^1 \varphi^* dy^* = \frac{\mathrm{Li2}[1 + A_S e^{-2N_\varkappa}]}{2N_\varkappa} - \frac{\mathrm{Li2}[1 + A_S]}{2N_\varkappa} + \frac{\mathrm{Li2}[1 - A_S]}{2N_\varkappa} - \frac{\mathrm{Li2}[1 - A_S e^{-2N_\varkappa}]}{2N_\varkappa} = \frac{\widetilde{Li}}{2N_\varkappa} \quad . \tag{6.50}$$

Obviously, the velocity profile, as given by Eq. (6.12) is again influenced by the gradient of the overpotential in the vicinity of the walls. In the case of vanishing pressure drop the fluid can be driven by the electric field of strength E_0 with an electro-osmotic mobility (6.23) given by

$$\mu_{eo} = \frac{\varepsilon\varepsilon_0}{\rho\nu}\frac{2kT}{ze}\left(\frac{\widetilde{Li}}{N_\varkappa} - \ln\frac{1+A_C}{1-A_C}\right) \quad . \tag{6.51}$$

As indicated by Manz, Harrison, Verpoorte, Fettinger, Paulus, Lüdi and Widmer (1992) for example, flow velocities for a $0.01M$ solution of up to 1 mm/s can be achieved with field strengths of the order of 100 V/cm. Fig. (6.5) illustrates the effect of the electric field on the mobility of a monovalent aqueous solution as a function of its concentration.

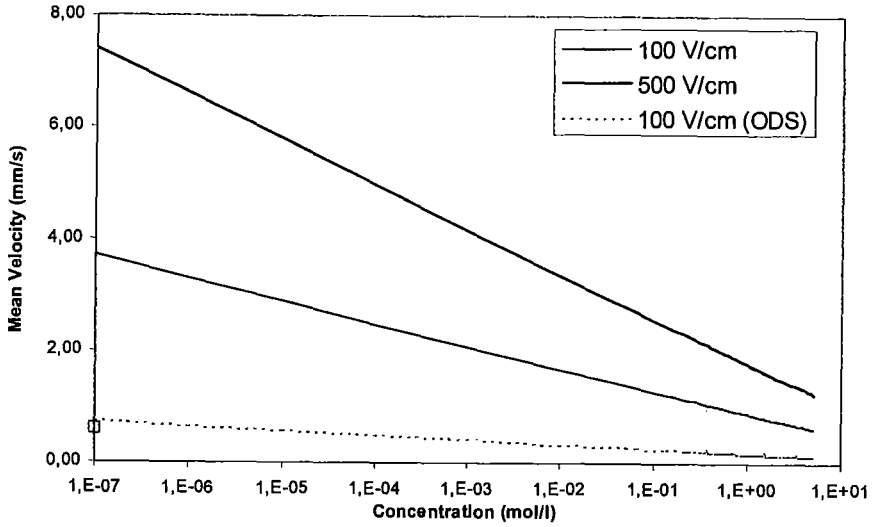

Figure 6.5: Effect of the electric field on the mobility of a NaCl solution in an open-tubular pyrex capillary of 132 μm diameter as a function of the salt concentration. For electric fields of 100 V/cm the mobility in the limit of pure water is compared with a measurement of Tsuda et al. (1982). The effect of the Octadecylsilane (ODS) treatment of the glass capillary has been reported in Tsuda et al. (1978) and accordingly taken into account here.

6.2.2 Pressure Drop by the Self-Induced Axial Electric Field.

The velocity profile (6.12) of the liquid, together with the charge density as given by Eq. (6.34), again causes a streaming current I_s, given by Eq. (6.25). Inserting Eqs. (6.45), (6.34), (6.41) for the constant A_C in Eq. (6.25) and using the symmetry condition (6.3), yields after some algebra

$$I_s = -\frac{8zen_\infty a^2 \Delta p}{\rho \nu l N_\varkappa^2} \left(2\varphi^*(1) - \int_{-1}^{1} \varphi^* dy^* - N_E \int_{-1}^{1} \left(\frac{\partial \varphi^*}{\partial y^*} \right)^2 dy^* \right) \quad . \tag{6.52}$$

The second term of Eq. (6.52) is given by Eq. (6.50), whereas the third term of Eq. (6.52) can be written as

$$\int_{-1}^{1} \left(\frac{\partial \varphi^*}{\partial y^*} \right)^2 dy^* = \frac{N_\varkappa}{2} \left(\cosh\left(2\varphi^*(1)\right) - 1 \right) \quad . \tag{6.53}$$

As in section 6.1.2 the electric field of strength E_0 causes a conducting current I_e, which is defined by Eq. (6.27) and results under this non-linear approach in:

$$I_e = \frac{\lambda a \Delta p}{z e n_\infty l} \frac{N_\varkappa^2 N_E}{4} \quad . \tag{6.54}$$

In the case of no externally applied potential and non-conducting walls the conducting current I_e acts in the opposite direction of the streaming current I_s and both currents compensate each other following Eq. (6.28). Under condition (6.28) we get the strength of the electric field E_0, which is built up under a given pressure gradient. Using the scaling proposed under section 6.2.1 with Eqs. (6.13), (6.14) and (6.46) and introducing the dimensionless ratio of property data N_P as

$$N_P = \lambda \rho \nu \left(\frac{\varkappa}{z e n_\infty} \right)^2 \quad , \tag{6.55}$$

the condition (6.28) yields for the parameter N_E:

$$N_E = \frac{2\varphi^*(1) - \int_{-1}^{1} \varphi^* dy^*}{\frac{1}{32} N_P N_\varkappa^2 + \int_{-1}^{1} \left(\frac{\partial \varphi^*}{\partial y^*} \right)^2 dy^*} \quad . \tag{6.56}$$

In Fig. (6.6), N_E is shown as a function of $N_\varkappa$. With decreasing gap width the electric

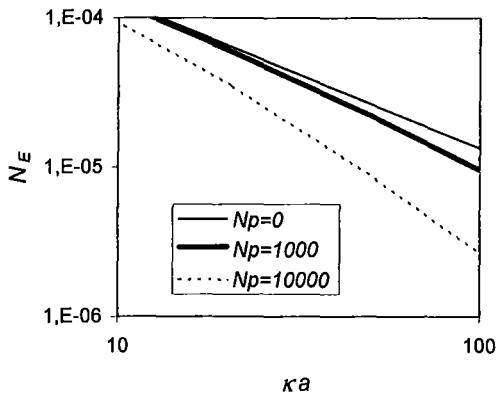

Figure 6.6: The dimensionless parameter N_E as ratio of electric to hydraulic forces in dependence of the dimensionless length ratio $N_\varkappa$ and of the property parameter N_P.

field in the microlayer is strongly increasing. Inspection of Eq. (6.47) with N_E restricted by Eq. (6.56) shows that

$$u^* = \left(1 - y^{*2}\right) - O\left(\frac{4}{N_\varkappa}\right) \quad . \tag{6.57}$$

With our assumption of $\varkappa a > 1$the influence to the microlayer effect on the flow is weak. Moreover the influence on the velocity becomes weaker if N_P becomes larger. Therefore

the microlayer effect is most pronounced for non-conducting liquids. If, on one hand, a potential is built up by a flow through a capillary and, on the other hand, such an electric field will drive the flow, we expect a kind of self-induction effect. The electric field, which is built up, will cause a secondary flow which is directed adversely to the main flow. As a consequence the pressure drop of the liquid flow through the capillary will be enhanced. Analogously as in section 6.1.2 with the Reynolds number of the channel $\mathrm{Re} = 2a\bar{u}/\nu$, Eq. (6.48) can be written in a dimensionless form we are used from classical fluid dynamics:

$$\frac{\Delta p}{\frac{\varrho}{2}\bar{u}^2} = \frac{24}{\mathrm{Re}}\frac{l}{2a}\left(1 - \frac{3}{2}N_E\left(\ln\frac{1+A_C}{1-A_C} - \frac{\widetilde{Li}}{N_\varkappa}\right)\right)^{-1} \quad . \tag{6.58}$$

Relation (6.58) allows us to predict the correction factor for the pressure drop over a microchannel. The last factor in Eq. (6.58) for the pressure drop over the microchannel can be interpreted as a correction factor for the pressure drop compared with that predicted by the Poisseuille flow theory:

$$f^{-1} = 1 - \frac{3}{2}N_E\left(\ln\frac{1+A_C}{1-A_C} - \frac{\widetilde{Li}}{N_\varkappa}\right) \quad , \tag{6.59}$$

This factor f is small but larger[2] than 1 in its range of validity for $N_\varkappa > 1$ and enhances the pressure drop compared with the pressure drop of a Stokes' flow.

6.3 Comparison with Experimental Data.

Figure (6.7) shows, however, that this correction factor f will not exceed 1% in the range of our approach, saying that the gap width is large compared with the EDL thickness. Even for non-conducting liquids f does not reach $0,01$ in microchannels with a gap width of $\varkappa a > 1$.

Mala and Li (1999) measured the pressure drop of water in a cylindrical capillary of fused silica. The measurements confirm that the pressure drop increases at small numbers $\varkappa a$. Mala and Li also performed similar experiments with water through a capillary of stainless steel. In that case they could not measure any pressure drop, as we can also explain with our theory. For stainless steel capillaries, with fully conducting walls, no electric field can be built up along the microchannel. Therefore $N_E = 0$ and no pressure drop enhancement is present.

Since careful pressure drop measurements in microchannels of sizes below 100 μm with water, aqueous solutions or liquid metals are scarce, we also looked into the pressure drop measurements over a small orifice by Hasegawa, Suganuma and Watanabe (1997). Even though these measurements are not exactly comparable, they confirm that the pressure drop increases indeed at small numbers $\varkappa a$.

Although our theory predicts the same tendency as the measurements by Mala and Li (1999) or Hasegawa et al. (1997) no quantitative agreement is obtained. Therefore the measurements of Mala and Li (1999) and Hasegawa et al. (1997) cannot be explained with this electrostatic effect.

[2]The second term of f^{-1} is positive because of the positive slope of the potential $\varphi(y)$ for $0 \leq y \leq a$.

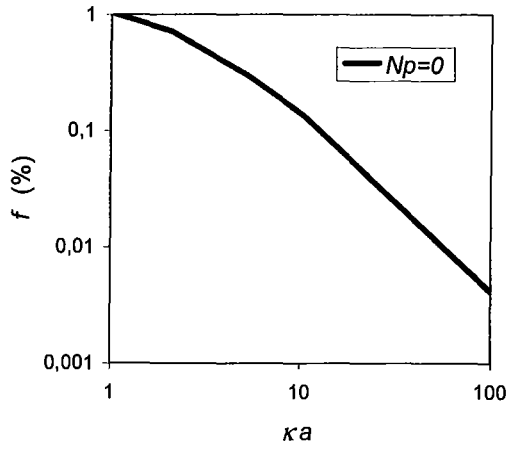

Figure 6.7: Pressure drop enhancement factor f for the flow of a non-conducting liquid through a glass slot.

6.4 Conclusion.

A new microscopic continuum model has been presented, which is based on the electric double layer theory of an electrolyte at an electrode. The good agreement between measured data and our predictions demonstrates the following major conclusions:

- Liquids may form an electric double layer at all kinds of surfaces, i.e. free surfaces and liquid / solid surfaces, even without electrodes and without an externally applied electric field.
- This electric double layer can be modelled assuming a surface charge density and a surface energy in a layer of zero thickness, which causes a Boltzmann distribution of point ions in a thin layer close to the surface.
- The simple assumption that this surface charge density and surface energy are the same for free surfaces, liquid / liquid surfaces and liquid / solid surfaces gives a good agreement with measurements of the contact angle and the electro-osmotic mobility.
- We could show under a nonlinear, analytical approach that a flow through a microchannel with electrically isolated walls causes an electric field which, in turn, increases the pressure drop at a given mass flow.
- All data needed for this model can be derived from known liquid properties, which makes the model easy to apply.

Bibliography

Abramowitz, M. and Segun, I. A.: 1968, *Handbook of Mathematical Functions with Formulas, Graphs, and Mathematical Tables*, Dover Publications, Inc., New York.

Adamson, A. W.: 1976, *Electrical Aspects of Surface Chemistry.*, 3rd edn, J. Wiley and Sons, chapter 4, pp. 216–228.

Bailey, A. G.: 1988, *Electrostatic Spraying of Liquids*, Electrostatics and Electric Applications Series, Research Studies Press, Taunton (England).

Blums, E., Mikhailov, Y. A. and Ozols, R.: 1987, *Convective Mass Transfer in Magnetic Field*, engl. edn, World Scient. Publ., chapter 4, pp. 205–258.

Chapman, D. L.: 1913, A contribution to the theory of electrocapillarity, *Philos. Mag.* **25**, 475.

Dahlkild, A. A.: 2001, Modelling the two-phase flow and current distribution along a vertical gas-evolving electrode, *J. Fluid Mech.* **428**, 249–272.

Dunken, H.: 1940, Über die Grenzflächenspannung von Lösungen gegen Quecksilber, *Z. physik. Chemie* **B47**, 195–219.

Frumkin, A. and Bagotskaya, J.: 1948, The potentials of falling drops, *J. Phys. and Colloid Chem.* **52**(1), 1–11.

Gouy, G.: 1910, Sur la constitution de la charge électrique à la surface d'un électrolyte, *J. Phys.* **9**, 457.

Grossman, P. D.: 1992, *Free-Solution Capillary Electrophoresis*, Academic Press, San Diego, chapter 4, pp. 111–132.

Hasegawa, T., Suganuma, M. and Watanabe, H.: 1997, Anomaly of excess pressure drops of the flow through very small orifices, *Phys. Fluids Letters* **9**(1), 1–3.

Helmholtz, H.: 1879, Studien über elektrische Grenzschichten, *Ann. Phys.* **7**, 337.

Hu, L., Harrison, J. D. and Masliyah, J. H.: 1999, Numerical model of electrokinetic flow for capillary electrophoresis., *J, Colloid and Interface Science* **215**, 300–312.

Israelachvili, J.: 1998, *Intermolecular and Surface Forces*, 2nd edn, Academic Press. 7th printing.

Landau, L. D. and Lifschitz, E. M.: 1973, *Theoretische Physik: Mechanik, Elektrodynamik*, Vol. 1 of *Theoretische Physik Kurzgefaßt*, Akad.-Verl. (Berlin).

Landolt-Börnstein: 1956, *Zahlenwerte und Funktionen aus Physik, Chemie, Astronomie, Geophysik und Technik*, Vol. 2, sixth edn, Springer Verlag.

Levich, V. G.: 1962, *Motion of Particles in Electrolytic Solutions*, 2nd edn, Prentice-Hall Inc., chapter 10, pp. 472–531.

Loman, R. and Zwikker, N. P.: 1934, The validity of Antonow's rule for the solid-liquid interface, and the consequent measurement of the surface tension of solids., *Physica* **1**, 1181–1201.

Lozada-Cassou, M.: 1992, *Fluids Between Walls and in Pores*, Decker Inc., chapter 8, pp. 303–361.

Mala, G. M. and Li, D.: 1999, Flow characteristics of water in microtubes, *Int. J. Heat and Fluid Flow* **20**, 142–148.

Mala, G. M., Li, D. and Dale, J. D.: 1996, Heat transfer and fluid flow in microchannels, *ASME DSC, Microelectromechanical Systems* **59**, 127–136.

Mala, G. M., Yang, C. and Li, D.: 1998, Electrical double layer potential distribution in a rectangular microchannel., *Colloids and Surfaces, A: Physicochemical and Engineering Aspects* **135**, 109–116.

Manz, A., Harrison, D. J., Verpoorte, E. M. J., Fettinger, J. C., Paulus, A., Lüdi, H. and Widmer, H. M.: 1992, Capillary electrophoresis on a chip, *J. Chromatography* **593**, 253–258.

Melcher, J. R. and Taylor, G. I.: 1969, Electrohydrodynamics: A review of the role of interfacial shear stress., *Ann. Rev. Fluid Mech.* **1**, 111–146.

Möller, H.: 1908, *Ann. Phys. (4)* **25**, 725.

Obot, N. T.: 2000, Toward a better understanding of friction and heat / mass transfer in micro channels - a literature review., *in* G. P. Celata (ed.), *Proc. Int. Conf. Heat Transfer and Transport Phenomena in Microscale (Banff)*, pp. 72–79.

Polat, M., Polat, H. and Chander, S.: 2000, Electrostatic charge on spray droplets of aqueous surfactant solutions, *J. Aerosol Science* **31**(5), 551–562.

Rayleigh, L.: 1892, On the theory of surface forces, II. Compressible fluids, *Philos. Mag.* **33**, 209.

Rice, C. L. and Whitehead, R.: 1965, Electrokinetic flow in a narrow cylindrical capillary, *J. Phys. Chemistry* **69**(4), 4017–4024.

Stern, O.: 1924, Zur Theorie der elektrolytischen Doppelschicht, *Z. Elektrochemie* **30**, 508–516.

Tsuda, T., Hibi, K., Nakanishi, T., Takeuchi, T. and Ishii, D.: 1978, Studies of open-tubular microcapillary liquid chromatography: II Chemically bonded octadecylsilane stationary phase, *J. Chromatography* **158**, 227–232.

Tsuda, T., Nomura, K. and Nakagawa, G.: 1982, Open-tubular microcapillary liquid chromatography with electro-osmosis flow using a UV detector, *J. Chromatography* **248**, 241–247.

Van der Waals, J. D.: 1893, *Thermodynamische Theorie der Capillariteit in de Onderstelling Van Continue Dichtheidsverandering*, PhD thesis, K. Acad. Wet. Amsterdam (Sect. 1).

Wolfram, S.: 1996, *The MATHEMATICA Book*, Wolfram Media, Inc.; Cambridge University Press.

Young, T.: 1805, An essay on the cohesion of fluids, *Philos. Trans. R. Soc.* **95**, 65.

Chapter 7

Appendix: List of Symbols

Fundamental Constants.

e	$1.60\ 10^{-19}\ C$	Electron charge
k	$1.38\ 10^{-23}\ J/K$	Boltzmann constant
ε_0	$8.85\ 10^{-12}\ F/m$	Permittivity constant

Scalars.

a	m	half gap width of the microchannel
A, A_S, A_C	$-$	constant of integration, giving the overpotential at the surface
f	$-$	pressure drop correction factor for microchannels
I_e	A	current due to the electric field over a conducting fluid
I_s	A	streaming current due to the fluid flow with its charge density
l	m	flow length of the microchannel
n_i	$1/m^3$	concentration of the ion set i
$n_{i\infty}$	$1/m^3$	concentration of the ion set i at infinity
p	Pa	pressure
q	C/m^2	surface charge density of the fluid
q_W	C/m^2	surface charge density of the wall
T	$°C$	fluid temperature
$\overline{u}$	m/s	fluid mean velocity
z_i	$-$	valence of the ion set i
ε	$-$	relative dielectric constant of the liquid
γ	N/m^3	surface energy of the fluid
$\gamma_{L1}^{(L2)}$	N/m^3	surface energy of the liquid 1 in contact with liquid 2
$\gamma_L^{(S)}$	N/m^3	surface energy of the fluid in contact with a solid
γ_0	N/m^3	surface energy of the nanolayer
φ	V	electric overpotential of the microlayer
Φ	V	macroscopic electric potential
λ	$1/\Omega m$	electric conductivity of the fluid
ν	m^2/s	kinematic viscosity of the fluid
ρ	kg/m^3	density of the fluid

ρ_{ci}	C/m^3	charge density of set i of ions
σ	N/m^3	surface tension
σ_{ik}^{el}	N/m^3	components of the electrostatic Maxwell stress tensor
θ	$^\circ$	static contact angle

Vectors.

$\vec{\mathbf{E}}$	V/m	electric field
$\vec{\mathbf{g}}$	m/s^2	gravitational field
$\vec{\mathbf{o}}$	m	position of the surface
$\vec{\mathbf{w}}\,(u,v,w)$	m/s	velocity vector
$\vec{\mathbf{x}}\,(x,0,0)$	m	coordinate vector
$\vec{\mathbf{y}}\,(0,y,0)$	m	coordinate vector

Characteristic Numbers.

N_E	$\frac{8zen_{\infty}l}{(\varkappa a)^2}\frac{E_0}{\Delta p}$	dimensionless ratio of electric to hydraulic forces
N_p	$\lambda\rho\nu\left(\frac{\varkappa}{zen_{\infty}}\right)^2$	dimensionless parameter with the fluid/wall properties
$N_\varkappa$	$\varkappa a$	dimensionless length ratio
Re	$\frac{2a\bar{u}}{\nu}$	Reynolds number of the microchannel
$\varkappa\,(1/m)$	$ze\sqrt{\frac{2n_{\infty}}{\varepsilon\varepsilon_0 kT}}$	Debye-Hückel parameter for symmetrically polyvalent solution